The nature of the crust of the Tallaringa Trough and Karari Shear Zone: a potential field analysis

Tim Keeping, 1037867

Contents

Abstract

The Tallaringa 1:250,000 map sheet defined by the South Australian Geological Survey Branch covers both Archaean and Palaeoproterozoic aged provinces of the north western Gawler Province separated by the ~700 km Karari Shear Zone. The Palaeoproterozoic geological domain northwest of the Karari Shear Zone covered by the Neoproterozoic Officer Basin is broadly classed as the Nawa Domain and further investigations are restricted to geophysical characteristics. Five magnetic domains have been interpreted, including the Tallaringa Trough which is bounded by the remaining four. Metamorphic characteristics of the four surrounding domains have been documented by dating techniques and REE analysis of drill core but ~1 km of cover sequence and a lack of outcropping basement have made geological interpretation of the Tallaringa Trough difficult. Using the combination of geophysical and petrophysical methods the characteristics of the magnetic domains are compared and two potential field forward models across the Tallaringa Trough are produced to reinterpret the domain boundaries and tectonic implications.

Introduction

The nature of the basement of the Western Gawler Province has become the subject of interest for the reconstruction of the Neoproterozoic Mawson continent and potential economic deposits due to its proximity with the highly mineralised Olympic Domain (Teasdale 1997; Daly et al. 1998; Betts 2000; Betts et al. 2003; Direen et al. 2005; Swain et al. 2005; Fraser and Lyons 2006; Hand et al. 2007). With few drill holes intersecting basement, cover sequences in excess of 1km deep and the lack of outcrop has required geophysical studies into the potential nature of its underlying basement. General domains in the northwest have been defined using magnetic interpretation but cannot be defined by the geological and geochemical techniques used to establish the domains within the Archaean – Palaeoproterozoic centre of the craton. Deep cover sequences and a lack of

outcrop have required the interpretive method of geometric potential field forward modelling has been increasingly applied to the area (Jessell and Valenta 1996).

The currently defined magnetic domains north west of the Karari Shear in the Tallaringa 250K map sheet are the Nawa Ridge Domain, Moondrah Gneiss, the south western section of the Mabel Creek Ridge and the superimposed Tallaringa Trough (figure 1). This study attempts to further refine the subsurface geology of the area by focussing on the area defined as the Tallaringa 1:250K map sheet by the South Australian Department of Minerals using the methodical classification of geophysical map patterns and testing the interpretations with potential field modelling. Previous studies have encompassed both large scale potential field models spanning the entire Gawler Province (Direen et al. 2005) and smaller scale interpretations taking a localised piece meal approach (Betts 2000; Betts et al. 2003).

The Tallaringa Trough study area is a Palaeozoic - Neoproterozoic epeirogenic basin where the shallow crystalline basement of four distinctive magnetic domains have been identified. The southern margin of the Tallaringa Trough coincides with the province spanning Karari Shear Zone (here on abbreviated to KSZ) which has been proposed to have experienced multiple reactivations and at least 80 km of strike slip displacement on its northern edge (Daly et al. 1998). The dip of the KSZ and its relationship with this smaller, rifted structure has been forward modelled using potential field data constrained by seismic and petrophysical data and map interpretation to ascertain the locations of the surrounding domains within the trough and therefore the nature of the trough basement.

Regional Setting

Geological Setting

The KSZ (figure 2) is a 800km long, southwest –north east curvilinear magnetic anomaly spanning the western Gawler Province where the Late Palaeoproterozoic Nawa Domain is juxtaposed against the Archaean the Early Palaeoproterozoic Christie Domain (Rankin et al. 1989; Betts et al. 2003; Direen et al. 2005; Fraser and Lyons 2006; Payne et al. 2006; Hand et al. 2007; Payne et al. 2008). On the south eastern side of the fault lies the sparsely exposed Christie Domain with a bland magnetic signature sitting strikingly against the highly magnetic KSZ that arcs south west from the northern Cooper Pedy Ridge and down parallel to the Tallaringa Trough in a sheared "boudinage" pattern of magnetisation (Benbow 1993; Direen et al. 2005). The generally low magnetic Tallaringa Trough is a Cambrian–Carboniferous-Permian aged depression within the Nawa Domain immediately north west of the shear zone. Its magnetic signature changes from low magnetic intensity next to Mabel Creek Ridge up to low to moderate intensity until the structure terminates at a fold in the magnetic texture. North west of Tallaringa Trough lies the generally moderate intensity Nawa Ridge Domain, running north north east up toward the Musgrave Block.

The crystalline basement of the Christie Domain comprises of Archaean aged rocks of the Mulgathing Complex which is a leucocratic, granitic, gneiss of metasediments metamorphosed to amphibolite grades (Hand et al. 2007). Originally deformed in the Archaean Sleaford Orogeny (2500 – 2400 Ma), sediments were later deposited proximal to the Archaean core of the province in a rift basin setting prior to the late Palaeoproterozoic Kimban Orogeny (Hand et al, 2007). This 1730 – 1690 Ma province wide orogeny produced a province wide shear zone system that has surrounded the Gawler Province with both the south eastern Kalinjala shear zone and western KSZ converging toward the northern Hiltaba/Gawler Range Volcanics domains (Hand et al 2007). The extensive regional effect of the Kimban Orogeny is recorded by metamorphism from the northern Peake and Denison and Mt Woods Inliers, upper amphibolite facies in the southern Fowler Domain and magmatism in the central domains (Hand et al. 2007; Payne et al. 2008).

The Nawa Domain lying northwest of the KSZ contains metasediments overlain by the thick cover of the Neoproterozoic Officer Basin. Monazite dating from sparse drill holes in the domain identified the granulite facies, high temperature assemblages were deposited during the late Palaeoproterozoic (Payne et al. 2008). Payne et al (2006) carried out U – Pb and Sm – Nd dating and REE analysis to determine the provenance of the metasediments and discounted the Gawler Province as the source and instead infers the most similar REE source as the far northern Arunta Region of the North Australian Craton.

Moondrah Gneiss, identified in the south west of the Nawa Domain, is a highly magnetic metasediment of mylonitised, granulite facies ferric and mafic metapelite gneiss (Hand et al. 2007). Two separate granulite assemblages have been identified, an earlier low P, high T event at ~1690 Ma producing spinel and cordierite, followed by an high P, high T assemblage of sapphirine and orthopyroxene at ~1650 Ma (Fraser and Lyons 2006). The later event is classified the Ooldean Event and adds a second, high temperature event to the basement in the southern Nawa Domain within ~40Ma of the regional Kimban Orogeny. Currently the Ooldean Event is presumed local to the Ooldea region but may be related by chronology with the comagmatic volcanism of the central St Peter Suite and Nuyt Volcanics (Daly et al. 1998).

Constraining the timing for the initial establishment and subsequent movements of the Karari fault are contentious. Fraser et al (2006) summarised the identification of two assemblages within Ooldea DDH3 by Swain et al (2005), one of only two holes drilled directly into the KSZ. Anhydrous, highly magnetite bearing granulite facies gneiss was EPMA monazite dated at ~1650 Ma, and mica from hydrous shear fabric of quartz-muscovite ± biotite Ar^{40}/Ar^{39} dated at ~1440 Ma (Swain et al. 2005). The former is interpreted as correlating to the timing of the juxtaposition of the Nawa and Christie Domains during the Ooldean Orogeny (1650 Ma). However the monazite dating of nearby Ooldea DDH 1 in the Moondrah Gneiss which also returned Ooldean Event age has been re evaluated [Dutch, pers. comm.] to be ~1700 Ma and there is the possibility

that the same analysis applied to the nearby Ooldea DDH3‘s age may result in ages related to the older Kimban Orogeny. This would strengthen the conclusion of Payne et al (2008) that Gawler Province wide, late Palaeoproterozoic shear structures were established by the end of the Kimban Orogeny. Reanalysis of Ooldea DDH2 also returned an Ooldean Event age which leaves future dating analysis of the Ooldea DDH3 core from the KSZ to constrain the timing of initial faulting on western edge of the Archaean core.

The shear zone separating the Christie and Nawa Domains was initially named the Karari Fault Zone by I.J. Townsend in 1971 (Milton 1974) and since has been interpreted by Teasdale (1997) as a dextral, and later Betts (2000) as a sinistral transform fault contact between the Gawler and Musgrave Blocks. Two metamorphic fabrics have been related to the Kararan Orogeny (Table 1), a term that has been used for events that produced regional high temperature and ultra high pressure across the north and western regions. A major influence in the classification had been the spatial difference between interpreted samples with ages that are chronologically separated by the voluminous comagmatic Hiltaba Event (1585 Ma). Betts (2003) classed the Early Kararan Orogeny as subduction on the western edge of the Gawler Craton during or immediately post Kimban (1690 – 1670 Ma), and the Late Kararan as a northern edge event involving the Cooper Pedy and Mabel Creek Ridges (1565 – 1540 Ma). Monazite dating by Payne et al (2008) confined the Kararan Orogeny to 1570 – 1555 Ma, and constrains earlier metamorphism and structures of the Early Kararan Orogeny to the Kimban Orogeny (table 1).

The second ~1440 Ma age identified in Ooldea DDH3 by Swain et al (2005) marks the minimum age when the shearing event cooled below amphibolite temperatures. Although Fraser, et al, (2006) considered the possibility of an extended cooling time until the argon isotopic system closed, the lack of similar extended cooling evidence in the Nawa or Christie Domains implies a shearing event could have occurred as late as ~1440 Ma. The Tallacootra and Coorabie shear zones east of the KSZ, have similar minimum aged Ar^{40}/Ar^{39} dated micas (1440 – 1460 Ma) and

both run parallel to the Karari fault. The three shear zones define the boundaries between basement domains in the western Gawler Province and connect along the Karari fault at the Cooper Pedy Ridge in the north. Fraser, et al, (2006) proposed reactivation of all structures as shear zones at ~1450 Ma but the error margin left open by dating constraints can accommodate the movement of structures occurring within the earlier Kararan orogeny (Payne et al. 2008). Two more metamorphic events are also implied by apparent argon isotopic loss during 1350 – 1320 Ma and 1200 Ma but there is no current regional evidence connecting the events to in situ mineralogy.

On the northern splay of the KSZ that bounds the Mabel Creek Ridge, Cooper Pedy Ridge and Christie Domain, sinistral transpression during the ~1200 – 1100 Ma Grenville Orogeny has been inferred by the magnetic structures (Betts 2000). Up to 80 km of movement along the shear zone has been inferred from apparent magnetic offsets in the Cooper Pedy Ridge that sits within the shear zone yet there is no metamorphic evidence recording such an event.

The western Gawler Province demonstrates over 500 Ma of protracted tectonic activity on and around the KSZ that lacks a high grade metamorphic record and has contradictory kinematic indicators. Both sinistral and dextral movements have been deduced from core samples and geophysical interpretations of trends that cannot be verified by crystalline outcrop. A westward migration and north – south to east – west rotation of deformation within the province after the Kimban Orogeny has superseded previous models based on complex terrane accretions (Payne et al, 2008).

Tectonic hypotheses point to the Nawa Domain being involved in convergence of two Palaeoproterozoic cratons, the SAC (South Australian Craton) and NAC (North Australian Craton). However, which craton was it part of and the tectonic setting are undefined. Payne et al, (2006) related the REE enrichment patterns of the Nawa basement to sediments from the NAC

and lower Willyama Supergroup of the Curnamona Province. Potential palaeocontinent reconstruction models of Betts and Giles (2004) and Wade et al, (2006) which both propose the SAC converging onto the NAC were also summarised as spatially plausible with temporal or geometric drawbacks. The Betts and Giles model proposed rotation of the now western edge into the NAC and WAC (West Australian Craton) to account for later (>1450 Ma) shearing from north to west.

Basin History

The basinal history of the Tallaringa Trough spans back to the Neoproterozoic epoch and is considered syn depositional and continuous with the Stuart Shelf and Adelaide Geosyncline cratonic sediments of the Adelaidean Period (850 – 570 Ma) (Drexel et al. 1993). The trough has been the marginal section of three unconformable Pre Cambrian and Palaeozoic basins and with the known metamorphic ages of proximal rocks dated no earlier than 1450 Ma, timing of the tectonic history has been restricted to seismic, palynological and indefinite sedimentary evidence. The western Officer Basin marks the initial tectonic deposition, corresponding with widespread rifted accommodation of the Marinoan chronostratigraphic unit of the late Adelaidean period. Significant deposition concluded in the Tertiary period with the both the Southern Rift system producing the Eucla Basin and uplift of the Stuart Range to the north, which generated the Garford and Tallaringa palaeochannels. Minor tilting and rifting recorded in both seismic sections (figures 4a & 4b) imply the area may have experienced epeirogeny during or post the formation of the Ackaringa Basin in the Carboniferous period.

Eucla Basin

The surface of the Tallaringa Trough is a gently dipping palaeodrainage channel cover of Quaternary sheet sands and dune fields of the Great Victorian Desert that drop only 120m over the 150 km from the adjacent northeastern Cooper Pedy Ridge to the Barton Sand Range in the

southeast (Benbow, 1993). Structurally the dip is controlled by the northern Stuart Range, and dips south to the local base level that hosts playa salt lakes in the top few metres of Tertiary sediments. Near surface sediments are both aeolian and alluvial in origin and vary from argillaceous to carbonate muds. Beneath the base level in the south west lies the mixture of the transgressive Tertiary Eucla Basin estuarine, palaeochannel bedload and aeolian sediments of sand, silt, clay and carbonates. The formations within the study areas are the Miocene – Pliocene Garford Formation and have both allochthonous and autochthonous characteristics (Benbow, 1993).

The formation follows a cycling eustatic pattern of transgressive marine carbonates over terrigenous sediments, then lignite at the highstand followed by progradation (Huo, 2000). It reaches it deepest within the Tallaringa Trough (15m) with alternating terrigenous and green sands, and carbonates in an estuarine setting, with correlations to units in the adjacent northern Giles and eastern Cooper Pedy map areas (Gatehouse, 2002). Supplying the alluvial components of the Eucla Basin were the northern Tallaringa and eastern Garford Tertiary palaeochannels. Both were structurally activated by the uplift of the northern Stuart Range in the Eocene resulting in the terrigenous sediments entering the Wilkinson Estuary of the Mallaringa Embayment. The Garford Channel contains outcrops of the Archaean Mulgathing Complex. Dendritic drainage from the eastern Challenger Domain into the Garford Channel may account for the low gold presence in calcrete sampling within the trough (Gatehouse, 2002). Underlying the Garford Formation lies the Eocene to Oligocene Pidinga Formation of sand, silt, clay and minor lignite bedload derived from the palaeochannels flowing southwest into the estuary.

Ackaringa Basin

The Ackaringa Basin dates from the Late Palaeozoic to Early Mesozoic eras and contains poorly sorted, conglomerate sediments due to glaciation during the Carboniferous and Permian eras. The

basin spanned an estimated 80,000km^2 including the Gawler Province, particularly in the series of Phillipson, Wallira and Tallaringa troughs straddling the northern curvilinear edge of the KSZ (Benbow 1993).

The Boorthanna Formation is the only recognised formation of the Ackaringa Basin within the Tallaringa Trough. The formation marks an unconformity with the glacially derived sediments of the Early Palaeozoic and pinches out to the southwest (Benbow 1993; Gatehouse et al. 2002). Palynomorphs of the Mesozoic era have been recorded but the layers are assumed to have eroded after either regression or continental uplift and accumulated in the subsequent exposure to the elements. Originally interpreted as Observatory Hill Formation it was reinterpreted geologically by Benbow and seismically by Cockshell (Benbow 1993). The addition of Permian palynomorphs identified by Rowett in sediment and detritus similar to the formation implied the formation was not terminated at the KSZ and hence considered part the more extensive Boorthanna Formation (Benbow, 1993; Gatehouse, 2002). Inspection of Wilkinson 1 revealed detritus from the Gawler Range Volcanics is implied by traces of volcanic porphyry and traces of limonite at the formation base (~210m mark) that would have required a supergene enriched source.

Officer Basin

The Neoproterozoic to Palaeozoic Officer Basin comprises up to 5 km of sediments separating the west of the Gawler Province and Musgrave Block. The basin structure is considered thick skinned with an east west orientation of lithospheric rifting implied by its negative gravity anomalies (Drexel, Priess et al. 1993). It is considered syn sedimentary with the Adelaide Geosyncline and Stuart Shelf to the east until the Cambrian – Ordovician Delamerian Orogeny uplifted the eastern Adelaide Geosyncline while the Officer Basin continued accumulating deposition until the Devonian period. It is the deepest stratigraphic layer of the ~1km deep Tallaringa Trough and least defined due to its depth (figure 4).

The Officer Basin comprises the longest sections of both intra trough drill holes, Wilkinson 1 (over 600m) and Piglet 1 (400m terminated by the maximum drilling depth) with the Early Palaeozoic, basinal Ouldburra and Observatory Hill Formations. The difference between the formations is contentious by their similar overall mudstone and sandstone characteristics except for two small but distinct sedimentary episodes. A chert layer in the north western Observatory Hills and the Ouldburra's thin layers of dolomite, halite and hydrocarbon demonstrate different Palaeozoic sedimentary histories in chronological similar layers within the same platform. The Central Basin Ridge lies between the formations and previous interpretations have recorded the two formations as being intertongued. Inspection of Wilkinson 1 by Gatehouse (2002) also noted the lithology as similar to the Boorthanna Formation.

The deepest identified stratigraphic layer drilled within the Tallaringa Trough is the Relief Sandstone, containing large crystallised halite layers intercalated with siltstone and sandstone starting at around 700m depth in Wilkinson 1. The complicated distinction already mentioned for the overlying layers continues between the Observatory Hills Formation and the Relief Sandstone which have been described as diachronous from comparisons with relatively shallow drilled cores taken throughout the trough by BP Minerals (Benbow 1993). These geological similarities and seismic interpretations may indicate tectonic movement during a transgression or regression. Confusion further arises to the north west where Relief Sandstone in Wilkinson 1 was interpreted as conformable beneath the Ouldburra Formation instead of the expected Observatory Hill Formation (Gatehouse, 2002). This may simply highlight differing opinions and the definition of all layers is subject to current and future exploration of the Officer Basin and neighbouring Musgrave Block.

Adelaidean sediments are inferred below the Relief Sandstone from drill core taken from drill holes in neighbouring and Adelaidean related domains (Benbow 1993; Drexel et al. 1993). The

Murnaroo drill hole in the Officer Basin in the far north west corner of the Tallaringa map sheet is separated by the Late Palaeoproterozoic Nawa Ridge. The drill core's stratigraphy infers the Proterozoic Adelaidean Rodda beds and Murnaroo Sandstone lie below the above identified formations. The Rodda beds are recorded as Marinoan glacial sheet derived conglomerates and limestones that have been measured at 2.7 km deep northwest of Tallaringa and observed in outcrop as far north as Marla (Benbow, 1993).

Tallaringa Trough

The Tallaringa Trough's geology and structure are subject only to limited drill holes and geophysical speculation so far, predominantly from the work of Finlayson (1979) and Gatehouse (1979) and both are heavily referenced in the Tallaringa Explanatory Notes and 250K map sheet (Benbow 1993). B.E. Milton (1974) suggested the depression is due to a half graben structure dip slip down the Karari fault. Finlayson (1979) used magnetic, radiometric, gravity and seismic data to interpret the Tallaringa Trough for department's 250K map sheet as a narrow, in filled structure bounded on the south east by the Karari fault and to the north west by a dip slip fault on the Nawa Ridge. Finlayson also interpreted the a basement ridge sitting northeast of the Wilkinson Lakes that cross cuts northwest – southeast, thus separating the trough into northeast and southwest sections. However, the prevalence of contiguous Carboniferous – Permian sediments throughout the structure do not reinforce such a structure capable of limiting deposition from either direction. All Cambrian sediments appear spread over the minor basin with the only likely changes noted in the south west where the Boorthanna Formation pinches out.

Timing of the minor rifting though is limited to relative events. Inferences of Cambrian aged activity in the trough are sourced from the basin sediments and seismic layers. Seismic interpretation by Cockshell reinforced a graben as the current description of the trough between the topographically higher Nawa Ridge and Christie Domains (Benbow 1993). The

Neoproterozoic Gardner dike intrusion shows no sign of displacement across the north of the KSZ. Aside from normal faulting of the basement and syn rifted overlying layers in the seismic sections there is no local evidence of any significant events after the onset of the Officer Basin. The trough is proximal to two similar troughs running along the southern splay of the KSZ south of the Cooper Pedy Ridge, but on the eastern Christie Domain side of the KSZ. The minor reactivation of the fault with respect to the creation of the trough appears to be localised tectonism attributable to movement in minor faults likely to have formed prior to ~1450 Ma.

Previous Models

Estimates of the dip of the KSZ are subject to where the study is taken. One of the longest continuous structures in Australia, the shear zone is poorly exposed and interest in has been restrained by the ability to construct computer models. Several geophysical derived interpretations have been made in recent years. Direen et al, (2005) modelled all the north west dipping shear zones in the central to north west of the Gawler Craton at 75°, including the KSZ. Betts, et al, (2000) study of the splayed northern section of the KSZ of the Cooper Pedy and Mabel Creek Ridges and Mt Woods Inlier, combined with areal field readings estimated a steep, sub vertical northern dip. Recent implementation by PIRSA of the multi scale edge detection technique known as worming has produced magnetic estimates along the Tallaringa Trough of 87° dipping south east (Heath et al, 2009). This finding highlights the problem of defining the dip according to which site is being assessed by the technique.

As for the nature of the crust undercover, the surrounding basement is reasonably well defined by drill hole data (Fraser and Lyons 2006; Payne et al. 2006; Payne et al. 2008).. The magnetic domains bounding the trough are the southern Moondrah Gneiss, western Nawa Domain, northern Mabel Creek Ridge and the eastern Mulgathing Complex (figure 2) Except the for Mulgathing Complex of the Christie Domain, all have similar assemblages of homogenous

provenance. Open seismic survey files and new geophysical techniques can provide depth to basement to aid in establishing local constraints to model the area by its petrophysical properties.

Methods

Petrophysics and Sample Descriptions

Available Data

SA Geodata

SA Geodata is the South Australian Government's electronic repository for geological, geophysical, and geochemical data across the state. Data capture has been continuous since the early 1990s within the Department of Primary Industries and Resources of South Australia (PIRSA), inputting geological and geophysical surveys, surrendered company reports, archived cores and other information into the database. Electronic copies of the sources are also kept for retrieval, and recently, an automated geochemical analysis program named Hylogger^{tm} has been implemented to further analyse, and re examine archived drill cores at the department's core library. Periodic snapshots of this extensive, state wide data set has been integrated with Geographic Information Systems (GIS) databases to enable visual research tools and the current internet portal (SARIG) for querying and downloading open reports and surveys (www.sarig.pir.sa.gov.au).

This extensive database was queried to locate information on existing drill cores and samples located within the provinces of the Nawa and Christie Domains, or Tallaringa Trough. Selection was then refined for proximity to two seismic traverses across the Tallaringa Trough and KSZ (figure 1).

Aeromagnetic and Gravity surveys

Geophysical survey data taken from the PIRSA survey database are summarised in figure 5. The gravity database consists of cumulative surveys amassed from company and department expeditions. As shown, density of gravity measurements is concentrated in company surveys in the southeast to northeast of the map sheet. Of note in the gravity map included in figure 5a is the wide gravity high within the sparse government gravity stations becoming noticeably narrower within a dense rectangular company survey. It is plausible that the wide gravity anomaly is narrower further south and therefore the assignment of some magnetic and gravity bodies in the final interpretation may be refined by more detailed surveys in the southwest of the Tallaringa map sheet. Both department funded aeromagnetic surveys (figure 5b) have a uniform 400m line spacing providing consistent resolution between the surveys.

Available Seismic Interpretation

In 1986, two seismic refraction and reflection surveys, were conducted across the Tallaringa Trough by CRA Exploration Pty Ltd and McBain for PIRSA (Benbow, 1993) (figure 4). 86AK-14 traversed the southwest of the trough from just inside the KSZ to the slope of the Nawa Ridge. It was coincident with the 1978 SADME drill hole Wilkinson 1, and the department used the survey path location to later drill the exploration well Piglet 1 in 1993 on the edge of a magnetic anomaly west of Wilkinson 1. 86AK-12 traversed south southeast to north northwest just north of centre in the trough, straddling extensive shallow drilling by BP Minerals and Shell Development Australia Pty Ltd.

Seismic horizons have previously been interpreted by D. Cockshell of SADME for the 1993 Tallaringa map notes, although the published interpretation is limited to only 4 km out of 45 km for both traverses (Benbow 1993). Open file SEG-Y files from PIRSA were viewed and interpreted in SeisSee™ for reflectors. Survey files were then imported into Gocad™ where primary reflectors defining the Eucla, Ackaringa and Officer Basins, and crystalline basement

were traced for the three dimensional coordinates that were input into Oasis Montaj – GM-SYS™ to build the potential field models.

Reports

The SA Geodatabase was used to locate much of the petrophysical data for forward modelling. As of writing, petrophysical logs have yet to be stored in the SA Geodata database in significant amounts so existing logs of Piglet 1, Wilkinson 1, and the LBR series were sourced from electronic or hardcopy archived reports in the PIRSA library (Barclay 1975; Finlayson 1979; Gatehouse 1979; Kay and Robson 1981; Morris et al. 1994; Gatehouse et al. 2002). Both magnetic susceptibility and specific gravity data were collected in relevant SI units (10^{-5} and kgm^{-3}). The specific gravity, density and neutron log are the three methods used to calculate density and result in the equivalent value. However, the three methods are not the same and do not all use the same units. But for the purposes of the modelling, all values are considered to be equivalent to SI kgm^{-3}.

Petrophysical data collection

Magnetic susceptibility and specific gravity for modelling constraints were largely collected from the PIRSA core library (NNL IL1 & 2, OBD 12, Piglet 1, Wilkinson 1, Ooldea 1, 2 & 3). Petrophysics was measured using tools provided at the core library; a Fugro GMS-2^{tm} magnetic susceptibility meter used in scan mode and set to 10^{-5} SI units. Specific gravity used digital scales modified with a connected harness within a water container. Although the device was accurate to one tenth of a gram, the decimal place was ignored for estimated uncertainty. Discrepancies between the data in reports and measurements made of Wilkinson 1 and Piglet 1 at the core library were identified and the most recent core library measurements were chosen over the

archived geophysical downhole logs. Drill holes that intersected basement are summarised in table 2 and figure 6.

Drill holes along the 86AK-14 traverse

OBD 3, 10, 12

The ODB drill holes were diamond drilled by Hammond Drilling Company for WMC between mid 1980 to late 1981 (Kay, et al, 1981). The operation targeted gravity and magnetic anomalies to assess for Mississippi Style mineralisation throughout the northeast trend of the Nawa Domain. In the company report 03887, out of 12 drill holes, all but one reached basement (OBD 10), and except for one generalised basement interpretation (OBD 3), all intersected a granite basement. Descriptions were limited to either white granitic gneiss or pink feldspar granite. Nine traverses of gravity and magnetic surveys were preformed prior to drilling and short magnetic wavelengths were targeted for shallow depths to basement. The true depth was consistently shallower than geophysical inference by between two thirds and one half of the inferred depth. The cited drill hole report is the stratigraphical and lithological source for PIRSA's SA Geodatabase referenced in earlier sections. Crystalline basement from drill cores OBD 6 and 12 have also been previously used to constrain the provenance of the western Gawler Province (Payne et al, 2006)

OBD 3 diamond drilled to 218m at ~10km north of the end of the traverse study, and intersected medium to coarse pink, gneissic granite at 131m. The basement occurred at near half the depth implied from the magnetic data. The magnetic susceptibility readings are low which imply a deeper source is responsible for the relatively high TMI compared to the bland neighbouring trough (figure 2). Drill logs describe shallow terrigenous Tertiary top layers unconformably overlying Permian sandstone with siltstones and conglomerates. Of geophysical interest are traces of pyrite recorded between 102 - 117m within the Permian layer which may slightly augment magnetic readings attributed to the granite basement. Basement in the PIRSA core library

recorded the variable but overall low susceptibilities averaging 2.48 x 10^{-5} +/- 2.51 SI, and average density 2948 +/- 43 kgm^{-3}.

Report 03887 records OBD 10 was drilled above where the Nawa Ridge descends into Tallaringa Trough and abandoned due to collapsing sand before reaching basement (Kay et al, 1981). To remedy this, OBD 12 was targeted west of ODB 10 into the Nawa Ridge to the south of the traverse and but intersected only 6m of crystalline basement at 464m. Traces of pyrite are recorded between 90 and 360m, generally at 2 - 5% and noted as 1 – 3mm sized balls between 260 to 360m. However the Fe sulphide is not assumed to significantly affect the magnetic intensity of the region. Basement is interpreted as granitic gneiss with quartz, feldspars and the magnesium mica phlogopite and susceptibility and specific gravity measurements averaged 2740 +/- 85 kgm^{-3} and 424 x 10^{-5} SI respectively.

Wilkinson 1 & Piglet 1

These drill holes are stratigraphic wells and are used to constrain the sediment stratigraphy of the Tallaringa Trough into the Boorthanna Formation, Ouldburra Formation and Relief Sandstone (figure 4b). Wilkinson 1 and Piglet 1 are the only drill holes within the southern central Tallaringa Trough and both were targeted over the hanging wall of the KSZ by the then Department of Minerals and Energy to investigate lignite and halite beds due to the Garford Palaeochannel (Gatehouse 2002). Weak, ferricretes and iron weathering from Observatory Hill in the Tertiary Mujena Formation were analysed for palaeomagnetic dating and pyrite is detected to variable levels throughout the Nawa Domain and Tallaringa Trough drill holes.

Magnetic susceptibility for the Wilkinson 1 core has been measured three times including for this paper and the results vary. Gerdes (Appendix 10, Gatehouse, 1979) recorded a variably susceptible core in c.g.s. units with higher readings in the upper 200 – 300 m halites of the

Ouldburra Formation and consistently higher susceptibility in the Relief Sandstone below 550 m. Gatehouse (1999) remeasured in S.I. units and found significantly lower values at the shallow depths of the halites but the same pattern in the Relief Sandstone. Gatehouse also compared these results with Relief Sandstone core from drill holes located west of the Tallaringa map sheet and found similar susceptibility in the same stratigraphic layer. However, measurements made at the PIRSA core library for this paper returned zero susceptibility at almost every 10 m interval throughout the core. Results were so generally low that the data mean of 0 could not register on the logarithmic graph of petrophysical results (figure 6). Since Gatehouse (1979) remeasured the Wilkinson 1 core personally this discounts the possibility that second higher values were due to geophysical downhole logging techniques detecting ambient magnetism and implies that the instruments used are the probable difference.

Piglet 1, which was drilled on the edge of a magnetic high, also registered a very low susceptibility rarely above 0 x 10^{-5} SI units. Traces of pyrite are associated with Ouldburra Formation clay descriptions but not with the large grain sizes noted in the OBD holes. Specific gravity registered 2398 +/- 124 kgm^{-3} but susceptibility results only averaged 3 x 10^{-5} SI and are not included on the logarithmic scale used.

LBR 20, 21 & 40

In 1993 the Department of Mines and Energy, South Australia (MESA) drilled 184 reverse circulation drill holes in the Barton map area south of the Tallaringa Trough to investigate mineral potential in the western Gawler Craton (Morris, Hill et al. 1994). Crystalline rock was intersected within 110m in 146 of the drill holes and the shallowest at only 9m, demonstrating the shallow nature of the Archaean Christie Domain. Geological and geochemical logs were performed on the core and radiometric and geophysical attributes were measured at 2m intervals. Using previous aeromagnetic surveys, the MESA Drilling Branch targeted the strongly magnetic,

short wavelength features in an area recognised for mafic and ultramafic dyke plugs. The drill holes were chosen initially by if they lay within the large magnetic subdomain of high frequency, low amplitude anomalies trending north into the Tallaringa map sheet. An overall petrophysical impression of the Christie Domain could be estimated since the three drill holes chosen for this study do not lie directly on high intensity magnetic anomalies.

Basement intersected by the LBR drill holes varied between the granulite facies Mulgathing Complex of the Archaean and Palaeoproterozoic Sleaford Orogeny (2500 – 2400 Ma), and amphibolite facies of the Lincoln Complex of the Late Palaeoproterozoic Kimban Orogeny. Crystalline rocks in LBR 21 (535 x 10^{-5} SI) and 40 (104 x 10^{-5} SI) are plutonic monzodiorite and granodiorite, and LBR 20 (11 x 10^{-5} SI), whilst only described in the report as biotite and feldspar amphibolite has a mineralogy similar to the above granodiorite. The core is stored as cuttings and was unsuitable for specific gravity measurement.

Drill holes along the 86AK-12 traverse

OBD 1 and 4

The traverse for the potential field model extends the seismic line by ~20 km northwest into the Nawa Domain but there are no areal drill holes. Instead the closest are OBD 1 at ~15 km to the north and OBD 4 at ~30 km south (figure 1). OBD 4 sits on the edge of the apparent eastern limb of the Nawa Domain but was abandoned at 120m during drilling due to unspecified reasons before reaching basement. OBD 1 reached basement at 115m and is within a magnetically similar textured, contiguous magnetic body that intersects the north western edge of the model line. Using the implied geophysical similarity of all OBD holes for petrophysical purposes, the results of OBD 1 have been extrapolated to where the forward model line intersects the Nawa Domain

(figure 2). However, unlike the garnet bearing gneiss interpretation of OBD 12, OBD 1 has been interpreted to contain haematite and the secondary mineral chlorite, and quartz veining.

SDA and SDA WL & 608.1

The SDA series of holes where drilled by Shell Development (Australia) in 1975 a line across the central and northern Tallaringa Trough to test for economic coal deposits in the Cainozoic Pidinga Formation which was then assumed to be a Permian layer. Since the goal was only to test for lignite all holes are too shallow for geophysical purposes but have been used as a stratigraphic guide.

Minoil Services drilled the hole 608.1 to further test for lignite beds in 1980 directly following on from the results of the SDA wells. It was only drilled to 50m and is only useful as a stratigraphic guide.

NNL IL1 DDH2, NNL IL2 DDH1

Noblex N.L. targeted magnetic anomalies in the Garford Palaeochannel near the south eastern side of the KSZ (Dreverman and Reveleigh 1980) using ground magnetic and total count radiometric surveys performed with magnetometer and scintillometer. The radiometric results were concluded to reflect channel sediments and magnetic anomalies were targeted with diamond drill holes. Both intersected perthite – hypersthene - pyroxene granulite basement within the estimated depths of the magnetic survey, indicating a slow cooled intrusive with no foliation. Magnetite is most prevalent (~5%) in NNL IL2 DDH1 above the 178m for a highly variable 415 +/- 1209 x 10^{-5} SI and a density of 3095 +/- 674 kgm^{-3} (Dreverman, 1980). NNL1 IL DDH2 was interpreted with only ~1 – 2% magnetite (415 +/- 424 x 10-5 SI) and (2684 +/- 309 kgm^{-3}) reflect the highly silicious company description.

Drill holes of sampling adjoining basement domains

Ooldea 1, 2 and 3

Although these three drill holes are not within the Tallaringa map sheet the Moondrah domain extends into the map sheet in the south at the KSZ and Ooldea 3 is one of the only drill holes that has targeted a magnetic high on the KSZ. Similarity in magnetic texture and the alignment of large, linear gravity bodies implies a geophysical similarity between areas of the Tallaringa Trough and the Moondrah Gneiss. The Moondrah Gneiss is currently accepted as a sub domain of the Nawa domain that terminates the Tallaringa Trough's south west boundary. The overall moderately magnetic and dense domain contains highly magnetic linear features folded from north northwest to northeast around the tip of the Nawa Ridge under granulitic conditions.

These holes were drilled by SADME and initially reported in 1987 for the department (Parker 1987). The drill core has since been the subject of significant interest and the extensively mylonitic Moondrah Gneiss has been described as the highest grade metamorphic rocks identified in Australia (Teasdale 1997; Daly et al. 1998; Payne et al. 2006; Hand et al. 2007; Payne et al. 2008).

Ooldea 1 targeted a moderate magnetic anomaly and intersected ~6m of weathered basement that returned no magnetic susceptibility value. Ooldea 2 intersected 130m of coarse magnetite bearing mylonitic gneiss within a small, highly magnetic fold in the hinge. Ooldea 3 has an overall highly mylonitic, fine grain size unlike the coarse nature of the two holes away from the KSZ.

Ooldea 2 has been extensively analysed and two phases of mineral formation have been identified by SHRIMP U-Pb dating in Ooldea 2. The conditions of the initial mineral phase of Ooldea 2 during the late stages of the province wide Kimban Orogeny (1730 – 1690 Ma) formed in

temperatures > 900°C and pressure ~1000MPa. Magnetite occurs as coarse gains visible in hand specimen and haematite as micrographic texture within garnet under microscope (Payne et al. 2008). The localised ~1650Ma Ooldean Event then produced another high temperature (~800°C) but lower pressure (~500Mpa) granulite assemblage.

Tilt Derivative

Geophysical interpretation commonly utilises two separate methods that are derived from the Total Magnetic Intensity (TMI) grid to define the boundaries of magnetic anomalies. The First Vertical Derivative (1VD) aids in discerning the boundaries by amplifying the high frequency, short wavelength anomalies to highlight where the change in magnetic readings is highest (figure 7). The Auto Gain Control (AGC) of the 1VD is then used to scale the amplitude of all anomalies of magnetic change to the same resolution. (figure 8). The AGC is overlapped with the 1VD on the left and bottom edges in figure 8 to illustrate the effects of scaling. High frequency textures of the southern central anomaly in the Christie Domain have been diffused into large, single anomalies by the effect of applying a running average determined using all anomalies.

Another method of both highlighting and equally scaling points of magnetic rates of change without losing resolution is the tilt derivative (figure 9). The tilt derivative is a method applicable to TMI and Reduced to Poles (RTP) data for effectively discriminating the edges enclosing magnetic bodies by their points of maximum change (Verduzco et al. 2004; Lahti and Karenen 2010). The technique is defined from complex analytical signal equation (1), where the analytical signal is given by

$$A = |A|\exp(j\theta) \quad (1)$$

where,

A – Analytical signal

j – imaginary unit

θ – the angle of phase

The phase (θ) is then derived by

$$\tan(\theta) = (\delta T/\delta z) / (\delta T/\delta x) \qquad (2)$$

where,

δT/δz – first vertical derivative of TMI

δT/δx - first horizontal derivative of TMI

The tilt derivative changes the denominator that is used to derive the phase angle θ to use the absolute value for the horizontal derivative δT/δx:

$$\tan(\theta) = (\delta T/\delta z) / (|\delta T/\delta x|) \qquad (3)$$

With the denominator always positive in the new equation, the vertical derivative is the only component influencing the sign of the result. Combined with the tan function's restriction of calculations to between ± π/2, the points are also normalised resulting in all anomalies being equally weighted in display, similar to the AGC. Inflection points are where the vertical derivative changes it sign are equal to zero and can be interpreted as close to the edges of distinct magnetic bodies (figure 9a). By setting the edges to zero, the technique also allows suitable software to automate the contouring of the zero values into plausible geophysical polygons. Figure 9b shows the RTP with the tilt derived contours overlayed to demonstrate that the contours delineate anomalies with not just obvious anomaly edges but adjoining shapes of slight magnetic response that might normally not be included.

Domain Interpretation

Magnetic sub domains within the established geophysical domains were interpreted using a combination of maps: TMI, TMI Reduced To Poles (RTP), 1VD, Bouguer Gravity and contours

generated from the Tilt Derivative in ArcGIS™ and Geosoft Oasis™. Each map allowed faults, gravity and magnetic bodies to be identified and delineated into polygons that were assigned attributes to enable visual manipulation to produce an array of maps accentuating geophysical characteristics.

Each sub domain polygon was assigned a subjective value for five fields (table 3) as a systematic process of identifying boundaries and enabling later selection by attributes. The process is iterative, started by drawing large general domains and subsequently drawing smaller domains within the initial large domains. RTP is preferred for choosing boundaries over TMI since RTP removes the effect of latitudinal variations in magnetic field direction and more closely approximates the source's true location. Gravity can help define large, general bodies by delineating distinct geophysical packages if magnetic and gravity boundaries are coincident.

The range of magnetic and gravity readings were mapped with the spectrum assign linear minimum and maximum values in the Tallaringa mapsheet area. This exaggerated the display to fix the highest reading red and the lowest reading dark blue in both. Amplitude for both properties reflects the overall strength of the property reading within a traced body denoted its overall spectrum colour. Wavelength refers to the general texture of the anomaly ranging from sharp and detailed through to diffuse and bland and is generally related to the depth to magnetic basement. Texture refers to the pattern of the magnetic anomalies. Bodies are classified as linear, folded or non specific (variable) and the internal detailed patterns are listed in Table 2.

Each number assigned to a field is combined into a Geophysical ID number to aid in later visual manipulation of the interpreted map. Anomalies can be assigned colours according to single field values or to each possible ID number. A general purpose use is to generate a map that is split into distinctly coloured general sub domains and the smaller anomalies within each sub domain are then coloured with increasingly darker shades of the general sub domain colour. The effect is an

easy visual discrimination of the areas with distinct geophysical signatures and the structure local to each sub domain, such as folds.

Euler Deconvolution

Geophysicists with limited prior structural knowledge can make predictions of geometry and petrophysical properties below the surface using Euler's 2D homogeneity equation (4) to calculate the locations of potential field sources (Thompson, 1982; Reid, 1990; Barbosa, 1999, Reid, 2002;, Mushayanddebvu, 2003; Silva and Barbosa, 2003).

$$\Delta T(x, z) = A / r^N \quad (4)$$

- N:- the degree of homogeneity, also termed the structural index
- $\Delta T(x,z)$:- the magnetic field anomaly value at position x and z
- r:- radius
- A:- source of the magnetic field

Potential fields (such as TMI (ΔT) or a Bouguer gravity (ΔG) profile) are measurements at a distance r from the source A. The degree of homogeneity N controls the calculation of the distance away and changes according to the shape of the source A. Applying the partial differential equation (5) to the TMI field measurement can then constrain the location of the potential field source (5).

$$(x - x_0)\, d\Delta T/dx + (z - z_0)\, d\Delta T/dz = - N\Delta T(x,z) \quad (5)$$

- x,z:- the location of the field measurement
- x_0, z_0- the constrained location of the field source

- $d\Delta T/dx$, $d\Delta T/dz$:- the gradient of the field in the direction of x or z

The technique requires different degrees of homogeneity (N) for the different possible shapes of a source to determine the distance r. Field strength decays with increasing distance away from the source and this rate of decay depends on the assumed shape (table 4). For gravity, a gravitational field's strength from a sphere is expressed by the inverse square law as demonstrated by Newton's equation of gravitational attraction. Since the potential field distributes over the expanding surface area of the sphere $(4\pi r^2)$ the strength decays by r^2. If the source body is a cylinder the decay is only order of 1 $(2\pi r^1)$ since the potential field is distributed over a circle. The lower the exponent, the shorter the calculated distance from the point of measurement to source (Reid, 1990).

The results of Euler Deconvolution constrain the points and surfaces of magnetic change for a shape of the source ($N\Delta T$) at horizontal position (x_0) and depth (z_0) along a 2D profile. N, the exponent, which is also named the equation's degree of homogeneity, is named the structural index for geophysical purposes. The structural index is a constant exponent value for specific magnetic structures pre-determined by Thompson (1982) and further refined by Reid (Reid, 1990) (Table 4). Since N changes the TMI value, it can also be thought of as similar to a continuation process where the larger values tend to locate deeper points for z_0. Prospective structures it can help locate are dikes, the contact between two different units and the position and depth of the throw of faults. The recommended magnetic structural indices from Reid (1990) are used here: N = 0 for locating the depths of contacts and N = 1 for the positions of thin, monopolar dikes.

Further refinement of (5) isolates the field measurement from the regional magnetic field,

$$x_0\, d\Delta T/dx + z_0\, d\Delta T/dz + NB = x\, d\Delta T/dx + N\Delta T(x) \qquad (6)$$

where,

- *B*:- the regional magnetic field

Values for both $\Delta T(x)$ and x are taken directly from the 2D profile, leaving three unknowns x_0, z_0 and B requiring at least three equations to solve. Magnetic data at 100m intervals was processed with in windows with spacing sizes of 10 points to overdetermine to three variables. The limits the window size should be at least half the depth being interpreted for. Since previous depth to basement estimates along the same profiles range from 200m down to a possible 1400m, the spacing of points in the windows needs to be long enough to cover the largest depths and short enough to accentuate any shallow, high resolution bodies (Benbow, 1993, Gatehouse, 1979). The long wavelength anomalies are approximately 10km wide and therefore require a 10km window to satisfy possible large structures. The generic value of the geothermal gradient (25°C per km) calculates 500°C at 20km depth which nears the Curie temperature for most rock minerals. A 10km window length can cater for a 20km deep body as the maximum depth magnetics can be reasonably interpreted before the heat of burial surpasses the Curie Point.

Extended Euler Deconvolution

A rule of thumb for interpreting Euler Deconvolution has been to choose the structural index which produced the most tightly clustered set of solutions. The centre of the densest cluster gives the profile position and depth for the given index. However in a magnetic field analysis all structures are possible magnetic changes and multiple indices produce valid results. And an example of the depth estimate being proportional to the structural index is demonstrated in figure 10 where identical patterns from all five structural indices in a section of the 86AK-14 TMI profile have ~1 km difference.

Extended Euler Deconvolution improves results for the structural indices 0 and 1 by estimating dip, susceptibility change across a boundary and thickness of an anomaly. Equations 7 and 8

apply to the structural index 0 for a magnetic contact, and estimates the dip and susceptibility change over contact boundaries,

$$(x - x_0)\, d\Delta T/dx + (z - z_0)\, d\Delta T/dz = \alpha \sin(\beta) \qquad (7)\ SI = 0$$

$$(x - x_0)\, d\Delta T/dz - (z - z_0)\, d\Delta T/dx = \alpha \cos(\beta) \qquad (8)\ SI = 1$$

where α is a function of both susceptibility change and dip across a contact, and β is a function of the dip.

Barbosa, et al (1999, 2003) found that for each window analysed, plotting the calculated *x* position versus a window's central *x* position displays the *x* ranges of clusters for simpler viewing. Replacing the spray filled Euler Deconvolution cluster graph (figure 12) is a generally straight diagonal line of one to one correlation with small intervals of weak correlation that tend to either curve horizontal or vertical (figure 13). Barbosa interpreted intervals of correlations close to zero (horizontal) as strong locations of the magnetic change, and diagonal intervals reflecting little or no change in the field. Another correlation by Barbosa, et al (1999) that tests the structural index is the correlation of ΔT to the estimated base level *b* within a window. As with the above graphical technique, the correlation closest to 0 implies the least bias and therefore the strongest indication of the structural index.

Fitzgerald et al (2004) tested several different discrimination techniques and found that calculating results using multiple structural indices proved grossly unreliable and that priori knowledge is important for interpretation. When applied to known kimberlite deposits in Sheoak Hill, South Australia, the authors recorded 78,000 results in which almost all were of indices of 1 or less, too small for the known kimberlite structural index of 2. This was attributed to ambient high frequency noise and false data points produced by interpolation. By already knowing which

indices to restrict searching for, the outlier minority of the results were correlated to the known deposits identified and similar potential targets. Therefore, in the likely folded, sheared and rifted Tallaringa Trough, results are limited to the expected structures of contacts (N = 0) and possible thin dikes from Extended Euler Deconvolution (N = 1).

Potential Field Modelling Procedure

To establish the two potential field model lines state wide magnetic and gravity stations were imported into Oasis Montaj™ database format from which grids of all geophysical maps and subsequent composites were generated. Both seismic interpretations were imported from Gocad™ into database format with 10 – 20 km added to both ends of the seismic survey lines to define cross sections in GM-SYS™ that extended from the Nawa Ridge to Christie Domain. The SEGY files were converted to image files and assigned as background images overlain with the plotted reflectors to allow any necessary tweaking of primary reflection lines prior to converting from time to depth. The two potential field forward model lines used the TMI (nT) and Gravity (mGals) field lines as guides for constructing a series of polygons with petrophysical properties to match both field lines.

Since the gravity field is generally the smoother of the two geophysical fields and therefore satisfied by less polygons it was the first to be delineated since. The large gravity polygons were traced down to 40 km depth and allowed space for smaller magnetic polygons to be traced inside. Magnetic susceptibility polygons were limited to only 20 km depth where the temperature approaches the magnetism destabilising Curie point. Many smaller magnetic polygons were only traced to 5 or 10km to highlight the sensitivity of interpretations to the inverse cube law. This follows the relationship that the depth to a magnetic or gravity source will be in proportion to the width of the anomaly detected. Magnetics are especially sensitive to depth changes and are progressively weakened by the increasing geothermal gradient. Therefore the closer to the surface

an anomaly can be defined the more confidently it can be assumed to be within the anomaly's radius.

Averaged susceptibility and density readings of crystalline basement were assigned as properties to each polygon. It should be noted that potential field models rely heavily on the petrophysical contrast between polygons and end product models can be satisfied with different absolute property values or shapes. The intention of this study was to model a reasonable geological structure that could be related to interpretation of geophysical maps, Euler deconvolution results and prior studies of the Western Gawler Province.

Results

Petrophysical data

Petrophysical readings of crystalline basement from drill holes surrounding the Tallaringa Trough are summarised in figure 7 using box and whiskers plots stacked by drill hole in descending age of last known metamorphic event, except for the OBD holes of the Central Nawa Domain. The Palaeozoic sediments did not register any susceptibility and are not included. Drill holes have been grouped by geophysical domain.

Density

Results appear to vary significantly depending on proximity to the KSZ with the highest density readings (Ooldea 3, NNL IL 1 & 2) originating from the highest grade assemblages sourced on or near the KSZ. Large ranges accompany assemblages identified with multiple metamorphic events during the late Palaeoproterozoic to early Mesoproterozoic yet overall the inter quartile range is conservative. Basement core from the Nawa Domain in the OBD series of drill holes is tightly homogenous as per the near uniform geological description of potassium feldspar granitic gneiss

with significant low exceptions at OBD 9 and 11 fitting the gravity signature. Ignoring Ooldea 1 due to its shallow core of weathered crystallised basement, the Moondrah Gneiss increases in range towards the KSZ (up to 4838 kgm^{-3}) but drops slightly in overall density for a median 2856 kgm^{-3}. AM/PB core samples show a similar behaviour for drill holes nearing the intensely deformed Mabel Ridge on the north eastern KSZ boundary with a median of 2773 kgm^{-3}. The NNL cores from the Christie Domain showed the largest variance ranging from a minimum 1389 to a maximum 5122 kgm^{-3}, resulting in a median equal with the Nawa Domain, of 2691 kgm^{-3}.

Magnetic Susceptibility

Susceptibility measurements of the proximal crystalline basements in figure 7 reveal an overall similarity to the density measurements. Similar to the density trend, the highest individual measurements of the Moondrah Gneiss occur at Ooldea 2 within the large fold of the KSZ. The coarse magnetite in Ooldea 2 rendered the consistently higher values by two orders of magnitude with a median of 16980 x 10^{-5} SI compared to the 653 x 10^{-5} SI units of more variable Ooldea 3. Mabel Creek Ridge has its closest similarities with the Moondrah Gneiss in both variation and high readings. AM/PB 1 yielded the highest susceptibility of the study with 136500 x 10^{-5} SI units and a median of 606 x 10^{-5} SI.

The pattern displayed by the overall moderately magnetic Nawa Domain is identical to the density results. Results are varied but limited to ~100 or lower and the weakest with only overall median of 47 x 10^{-5} SI across the domain.

Measurements of the two very similar Late Palaeoproterozoic aged NNL cores from the south eastern side of the KSZ demonstrate much less susceptibility (combined median of 187 x 10^{-5} SI). The NNL drill cores are taken from the map area containing both the high frequency, moderately magnetic Mulgathing and bland Christie Gneiss and the samples therefore reflect measurements applicable to the Christie Domain at the potential field traverse 86AK-12.

Seismic Interpretation

Two previous seismic reflection and refraction surveys were interpreted to isolate the depth to crystalline basement in the Tallaringa Trough (figure 4a & 4b). To identify the primary reflectors progressive levels of auto gain control were used to highlight the strongest reflections. In both surveys, three major reflectors observed by Cockshell (Benbow 1993) defining the boundaries between the Precambrian basement, Cambrian Relief Sandstone/Ouldburra Formation, Cambrian Observatory Hills and Carboniferous-Permian Boorthanna Formation/Tertiary deposits. Two way times were converted to depth using constant interval velocities. The top two sediment layers were assigned velocities chosen from depth intervals previously determined by Finlayson in the well velocity survey of drill hole Wilkinson 1 (Gatehouse 1979). In the Wilkinson 1 and Piglet 1 cores the Cambrian lowest layer containing the undifferentiated Officer Basin and Adelaidean sediments appeared weakly aggregated than the variably carbonaceous overlying layers and therefore a significantly lower velocity was chosen.

86AK-12

Three primary reflectors are observed across the northern seismic traverse 4a. ~250 msec of vertical displacement occurs at trace index 311 where the Tallaringa Trough meets the Nawa Domain indicating the last major tectonic event occurred after the onset of the Carboniferous period. Patterns of small faults and slopes in the basement reflector are generally reflected in all reflectors except in the central to north western area. Permian scouring is suspected to have strongly altered the original horizon of the upper layer. Overall reflector stratigraphy is comparable with the southern section with the noteable exception that deepest displacement occurs on the Nawa Domain edge of the trough instead of the KSZ edge.

86AK-14

The seismic section of the southern most survey (figure 4b) shows the central Tallaringa Trough is a well bedded minor basin that has experienced episodes of extension throughout the Cambrian to Permian. The developments of minor rifts are demonstrated across all primary reflectors and demonstrate that the trough experienced ~1 – 2km of rifting.

Three significant vertical faults cross all primary reflectors in the 86AK-14 section indicating that the trough experienced its last major tectonic movement during the late Palaeozoic era. The largest extensional down throw occurs at the KSZ (the SE end) where two faults record a block that has displaced by ~150 msec since the onset of the Carboniferous (trace indexes 249 – 621 and 1551). Near trace index 5457 at the north western end the third vertical fault to cross cut all reflectors displays ~80 msec of displacement. A fourth major extension is observed where the Tallaringa Trough meets the Nawa Ridge (trace index 6697). appears obfuscated by near surface noise and it is unknown if the fault cuts the shallowest horizon. The vertical drop cannot register seismic reflections and prevents an accurate interpretation of the weak Carboniferous reflector. Cockshell (1993) relates structures in the central upper layer to Permian scouring consistent with the glacial origin of the Permian sediments which may have obscured the upper reflection. The basement horizon demonstrates ~150 msec of displacement which implies affinity with the ~150 msec displacement at the KSZ.

Results of modelling

Extended Euler Deconvolution was run multiple times on the magnetic and gravity profiles with an array of windows lengths of 10km, 5km, 2km and 1km, to attempt to accommodate the range of wavelengths from the longest field anomalies down to a window size that could isolate shallow

bodies (Reid, Allsop et al. 1990). Using GM_SYS™, the estimate *x* positions could be cross referenced with a 1VD and Tilt Derivative maps to reference the locations of magnetic change.

Results from running Euler Deconvolution Matlab™ scripts (supplied by G. Baines) are stored as separate tables for structural indices 0 and 1 (tables 5, 6, 7 and 8). For the magnetic results, whilst index 1 produced small, manageable tables of possible thin dike positions in all cases , index 0 (magnetic contact) produced a large set due to all changes in magnetism being possible contacts, irrelevant of the true structure. Following the suggestion to analyse by clusters of solutions (Fitzgerald, et al, 2004), and to cut hundreds of solutions down to a manageable number, each set of results was processed for averages and standard deviations of both standard and extended deconvolution *x* and *z* values, dip, susceptibility and count per cluster.

Gravity has been included but the small number of results from a small number of data points restricted analysis. After applying Thompson's acceptance tolerance (Thompson, 1982) results above a 1km window size were rare. Although the results can be considered weak they did provide possible indicators during the modelling process.

As indicated previously, the number of results depended largely on the window size and structural index. Thin dike analysis consistently returned a low number of results where as the magnetic contacts ranged to over 200. The larger the window size the larger the pool of acceptable results. These were reduced to averages and standard deviations for display purposes (tables 5,6,7 and 8). Graphical display of both indices for both potential field model lines are presented by window size in figures 12 – 20.

The numerous results pose the problem of which dip or structure to implement. Tightly clustered results of magnetic contacts can present dips with a range of over 100°. Susceptibility and dip changes registered many times within areas where the TMI readings were wide and smooth

anomalies. Confidence during modelling of structures was therefore taken by results that recurred at similar positions across window sizes and similar dip angles.

86AK-12

Magnetic contact (SI = 0)

Magnetic contacts in the 10 km wide window are strongest at ~23 km, ~43 km and at the KSZ (~60 km). However the depth estimates are significantly shallower than the seismic interpretation but how this effects the usefulness of generated locations of estimated points of magnetic change are unknown. Since the technique is commonly to estimate the depth to magnetic basement the results from all windows are treated with caution. The set of results derived from the 5 km window faired better with a greater range of depths displayed across the analysis. The depths derived from the seismic interpretation are only reasonably reflected at the ~25km and ~43 km locations though, implying only those specific results agreeable to the known structures. Although that majority of results can be treated as spurious and are taken with caution, those located between 0 – 20 km and 60 – 80 km did follow the known the overall shallow depths of the Christie and Nawa Domains.

Depth estimates appeared to improve with decreasing window width but the previously established basement topography is weakly matched by Euler deconvolution results with few points in any sized window. Results that repeat at a general *x* location are noted for possible structure modelling due to their consistency across the four windows.

Thin dike (SI = 1)

The relative scarcity of results for structural index 1 demanded a less rigorous elimination of results. In particular the KSZ was the only structure which attracted a strong cluster of results at 10 km window, registering as a near vertical dipping dike (figure 15). It repeats in the 5 km window but not in either the 1 or 2 km windows. In 2 and 5 large, tight clusters highlight variable (~50 - 60° mean dip) intrusions at ~42 km and ~52 km respectively indicating a general southeast dip to dike like structures in the central Tallaringa Trough.

86AK-14

Magnetic contacts (SI = 0)

Starting with the largest window (10km), the largest clusters occur at ~19 km (42 results) and ~34 km (64 results) (table 7). The first large cluster ranges of ~ 3 km and is highly varied in dip and susceptibility changes where as the ~35 km cluster is tight ~34 km in location, near vertical dip and susceptibility. Dropping the window size down to 5 km detected more individual contacts across the traverse and still retained the two previously mentioned contacts. The KSZ registers the largest cluster within this window but unfortunately the range of dips is nearly 180°.

At 2 km window size the number of contacts has increased with increased sensitivity to the shallower anomalies. The previous three strongest points of contact are included, implying they are deep structures that rise to shallow depths. The ~34 km contact is a again detected with a near vertical dip and the ~18 km anomaly replaced by two opposite dipping structures. Two clusters are located over KSZ implying a magnetic contacts have registered on both sides. This same general pattern recurs within the 1 km window. No large clusters are detected within the Christie or Nawa Domains in any sized windows. Instead both domains register patterns of very shallow, thin anomalies implying shallow folds.

Again, depth estimates are highly variable for all windows and rarely reflect known drill hole or seismic data and it has been assumed that anomaly consistency across window sizes are the best indicator for relating Euler results to the modelling process.

Thin dike (SI = 1)

A dike like structures is repeated across all window sizes at ~50 km on the 86AK-14 traverse. The estimate dip 40-50° is also consistent giving the strongest reading of the traverse. As shown in figures 12 – 16, the few other dike like structures are inconsistent and were not referenced for modelling.

Results of Forward Models

To compare the petrophysical properties of the underlying basement of the Tallaringa Trough with neighbouring domains, the Tallaringa 1:250,000 map sheet has been interpreted into eight geophysical sub domains by magnetic and gravity amplitudes, magnetic textures and wavelengths (figure 20 - The Cooper Pedy Ridge, Western Mabel Creek Ridge, Christie Domain, KSZ, Tallaringa Trough, Central Nawa Domain, Northern Nawa Domain and Moondrah Gneiss). The Nawa Domain has been divided by the apparent depth to basement (wavelength) into the shallow Central Nawa Domain and the Northern Nawa Domain which is covered by the Officer Basin. Mabel Creek Ridge has been labelled the Western Mabel Creek Ridge to differentiate the low gravity package from the high gravity domain referenced on the adjacent Cooper Pedy map sheet in literature (Benbow, 1993).

86AK-12

Central Nawa Domain (CND)

The short northwest Central Nawa Domain (here on CND) fits an almost mean Earth value of 2680 kgm^{-3} across the uniform, flat gravity response of the northwest. The lack of drill core on or near the potential field line required inference from a wide range of densities from the nearest OBD drill holes (figure 6). OBD 1 recorded a significantly higher density (2827 kgm^{-3}) than proved able to fit the model and the lower granitic value of 2680 kgm^{-3} lies closer to the statistical average for the cluster of proximal drill holes (OBD 1, 5 and 7) of 2689 kgm^{-3}.

The high frequency, low intensity magnetic characteristics are a contrasting boundary feature to the high frequency, high intensity of the adjacent Western Mabel Creek Domain. The abrupt ~400 nT change occurs at a triangular junction of NE-SW and NW-SE faults where the Nawa Ridge from the west, Mabel Creek Ridge from the east and a body similar to both from the north intersect. The area of exceptional low magnetism may be a remanent intrusion or a product of the multiple faulting that has destroyed the positive magnetism. Euler Deconvolution generated its strongest indicator at the position with the 10 km window as a magnetic contact which implied a deep contact boundary.

Western Mabel Creek Ridge Domain (WMCR)

The Western Mabel Creek Ridge Domain (here on WMCR) refers to the magnetic continuation of the Mabel Creek Ridge into the Tallaringa Trough highlighted by the tilt derivative (figure 9a). It is characterised by its high frequency, high intensity TMI response that stretches the NW length of the Tallaringa Trough in a low density package but originates from the high density package in the Mabel Creek Ridge (figure 19). The prefix *Western* is used to distinguish the low density package from the high density Mabel Creek Ridge of previous literature (Betts, 2000, Betts et al, 2003).

The underlying package modelled with almost the same the density (2690 kgm^{-3}) of the CND which raises the implication that the above area labelled the CND Domain may be part of the WMCR. The northern, elongate body that intersects the 86AK-12 field line adjacent to the WMCR has similar direction to the CND but contains two high magnetic anomalies that are similar in convoluted texture to the WMCR (figure 20). The difference between both domains has been argued using the magnetic fault marking a large change (~400 nT) in the magnetic intensity but it should be noted that other geophysical similarities leave the boundary definition open to interpretation.

Euler Deconvolution for possible structures favoured using magnetic contacts with few results for the thin dike intrusion. The WMCR is also defined as the trough long, continuous anomaly from inspection of the tilt derivative and therefore the cross section has been modelled as a single, folded body where the depth of the folded limbs dictates the TMI anomalies. The high frequency anomalies are dissimilar to the NW adjacent larger anomaly but are grouped by their geophysical similarity from interpretation (figure 20). The NW anomaly fitted a single, ~15 km wide, high susceptibility (9100 x 10^{-5} SI) polygon with shallow folds.

Tallaringa Trough

The Tallaringa Trough has been reinterpreted as the denser package between the WMCR and KSZ. The gravity graph in figure 21 displays a long, high amplitude anomaly within the Tallaringa Trough that tapers northwest which implies a wide high density body contacting the WMCR at a northwest dipping thrust fault. Adding the coincidence of the 900m deep trough with the gravity high distinguishes a higher 2740 kgm^{-3} density value.

The magnetic response of the Tallaringa Trough is a bland, low frequency and low amplitude response with one small amplitude anomaly that tapers NW. No structural indices returned strong

results above the ~55 km mark and by the geophysical interpretation, the tapering magnetic tail does not correspond to an anomaly crossing the line. The tail is therefore assumed to be produced by the anomaly adjacent to the field line, similar to an unmigrated reflection in 2D seismic processing. The high frequency wavelet has then been modelled in isolation as a shallow, thin, near vertical thin dyke.

Karari Shear Zone

The KSZ spans ~5 km on the 86AK-12 profile where the gravity response decreases to the profile's minimum of -30 mgals. The 10 km Euler Deconvolution window indicated a vertical dipping dike in the magnetic profile with a cluster of 22 results averaging ~80° dip at the ~58 km position (figure 18). All window sizes indicated a series of magnetic contacts at the same position (figures 14 – 18). Combined with a vertical fault at the SE edge of the seismic profile (figure 4a), a series of vertical dikes were modelled across the Tallaringa Trough and decreasing in density (2680 – 2620 kgm^{-3}) to the SE.

The sharp magnetic response of the KSZ could not be as neatly satisfied with the gravity polygons. Magnetic susceptibility values for the parallel dikes that fitted the gravity shifted the maximum calculated magnetic response ~2 km NW of the true anomaly. Attempts to translate the response using the variable dipping contacts implied by the results for magnetic contacts (Figures 14 – 18) failed to adequately accommodate both sharp the ~800 nT increase and ~1000 nT decrease.

Christie Domain

The Mulgathing Complex of the Christie Domain lies SE of the KSZ. To satisfy the long wave length of increasing gravity response to the SE required separate blocks to accommodate both the

deep low adjacent to the KSZ and high. The boundary between the KSZ and Christie Domain is undefined by the gravity response and fit the same low 2620 kgm^{-3} of the KSZ for ~10km into Christie Domain. The adjacent 2700 kgm^{-3} density value reflects the large high density body within the Christie Domain that runs parallel to the KSZ and extends SE until it terminates at the Blowout Shear Zone (Direen at al, 2005).

The magnetic susceptibility of both blocks modelled with two near equal values (300 and 310 x 10^{-5} SI) to fit the long wavelength, low amplitude TMI response. Both values within the first standard deviation for the constraining drill holes NNL IL2 DDH1 and NNL IL1 DDH2 (table 2).

86AK-14

Central Nawa Domain (CND)

The gravity response of the gneissic granite of the CND at the NW end of the field line consists of a long wavelength decreasing ~10 mgals in the SE direction to a minimum of ~20 mgals. The geophysically interpreted domain consists of two major magnetic bodies of high frequency characteristics that decrease in overall TMI until terminating at a magnetic fault ~3 km NW of the local gravity minimum. Using this magnetic position as the boundary for the CND fitted a homogenous block of above average granite density.

Western Mabel Creek Ridge Domain (WMCR)

The range of the WMCR cross section interpreted on the 86AK-14 profile lies in three places. The overall flat characteristics of the WMCR gravity contains two medium wavelength, low amplitude anomalies attributed to the intertongued Tallaringa Trough (figure 23). The significant sine wave with a ~650 nT decrease within the WMCR occurs near the vertical dip slip fault

identified in the seismic traverse (figure 4b). Initial attempts to model the major magnetic change at this position failed since the rift lies ~4 km SE of the centre of the anomaly. The model has used the results for multiple contacts with variable dip angles across the domain and a major contact traced to the 20 km model base (Figures 16 – 18). The SE boundary at ~35 km mark where all Euler Deconvolution windows indicated a near vertical contact.

Tallaringa Trough

In the profile the Tallaringa Trough is bounded by the magnetic contact at ~35 km and the KSZ. The large amplitude, long gravity wavelength fitted a body of 2740 kgm^{-3}, equivalent to the same domain in 86AK-12. The constraining petrophysics of the CND and WMCR required the magnetic susceptibility the distinctly lower 150 x 10^{-5} SI versus the 480 x 10^{-5} SI in the 86AK-12 profile. This may be due to a possible mix of domains in profile 86AK-12 since the domain is in closer proximity with the WMCR. A syncline has been modelled at the positions of the two prominent magnetic anomalies based on the possible remnants of an antiform or synform observed in geophysical interpretation.

Karari Shear Zone

The northern profile intersected the KSZ on an intense magnetic high where as the southern profile intersected a relatively low magnetic response between two characteristic highs perpendicular to the profile. The gravity response descends to a profile low of -25 mGals which fitted the average density of 2670 kgm^{-3}. The TMI reaches a maximum of ~0 nT before decreasing to ~-450 nT in a sine wave implying a magnetic contact at ~60 km. All Euler Deconvolution windows indicated two magnetic contacts and the results for the thin dike structural index for the 10 km window reinforced the near vertical dike model.

Christie Domain

The length of the southern profile within the Christie Domain contains two petrophysical blocks but is approximately half the length and limited to displaying only a small section of the second, higher density block. The same density values used for 86AK-12, 2620 kgm^{-3} and 2700 kgm^{-3}, satisfy the increasing long gravity wavelength on the 86AK-14 profile. Unlike the bland but relatively moderately intense magnetic profile of 86AK-12, the southern transect of the domain has very low intensity contains with high frequency magnetic anomalies of that increase in amplitude to the SE. Geologically, the anomalies are assumed to be related to the Lincoln Complex intrusions identified in the LBR drill cores south of the Tallaringa map sheet (figure 1). Euler Deconvolution detected the anomalies as shallow contacts and almost no thin dike intrusions SE of the KSZ. However moderately NW dipping dikes have been fitted

At ~10 km in 86AK-14 though, the overall magnetic response stays at ~0 nT which is similar to that of Mabel Creek interval in 86AK-12. This is also considered the point of faulting between the western Mabel Creek and central Nawa Domain. Due to the strongly homogenous nature of the Nawa Domain assemblages changes in susceptibility should be expected. Map interpretation by the tilt derivative (figure 20) shows a confusing zone of very close NE-SW faults either terminating at or displaced within the MCR body and may be a sign of movement in the trough post dating the compression of the Nawa Domain with the trough.

Discussion

The Tallaringa map sheet has been interpreted into eight sub domains by petrophysical, textural and apparent wavelength properties. Table 9 presents a simplified petrophysical summary of the domains and figure 19 displays the magnetic and gravity responses. Two new domains have been identified in the north west of the Tallaringa map sheet and the Tallaringa Trough appears to

share geophysical properties with two neighbouring domains by the results of the forward models.

The area northwest of the central high gravity anomaly in both field models share the low gravity and moderate to high magnetic attributes of the WMCR on the NW side of the Tallaringa Trough. The central high gravity anomaly coincides with low TMI responses similar to the two domains buried by the Officer Basin, the Moondrah Gneiss and Northern Nawa Domain in the NW corners (figure 19). By its petrophysical properties the trough has high density similar to both the Moondrah Gneiss and Mabel Creek Ridge.

From the 86AK-12 potential field model the differences in magnetic susceptibility across profile imply a lithological change in the centre of the profile. The wide, contiguous body highlighted by the tilt derivative that originates from the Mabel Creek Ridge Domain traces the length of the trough and modelled as a highly susceptible layer that has been distinguished from the Central Nawa Domain. The magnetic waveforms decrease in intensity and frequency as the body extends SW and has been able to satisfy short amplitude but relatively wide anomalies within the Tallaringa Trough. The underlying gravity signal is similarly low to the Nawa Domain but the magnetic characteristics are significantly stronger. The large body appears to be a continuation of the Mabel Creek Ridge but in a distinctly less dense package and therefore labelled as the WMCR.

The magnetic and gravity signature of the central body marks a change in geophysical nature. Bodies identified over the gravity anomaly are consistently lower in amplitude for the length of the trough (figure 19). By comparison the adjacent package identified by tilt derivative is moderate to highly magnetic. Wavelengths for the central body are inferred as deep, wide anomalies rather than the more remote possibility of clustered, high intensity, high frequency bodies forming larger, disjointed NE-SW orientated linear bodies for over ~300 km.

The folds and dip angles of the forward models imply that the uncorrelated Tallaringa Trough domain has either intruded into or been thrust over by the WMCR. Analysis of the Moondrah Gneiss by Teasdale (1997) found an 87° mineral lineation implying steep uplift on the NW side at the southern edge of the KSZ. Near linear geophysical features imply uniform NW – SE compression on the western edge of the KSZ with magnetic features displaying no significant movement in other directions.

Conclusion

By methodical geophysical comparisons the Tallaringa Trough displays partial characteristics of its north and south neighbouring domains, the Moondrah Gneiss and western Mabel Creek Ridge. Using the tilt derivative to identify boundaries of positive magnetic source bodies and assigning parameters based on visual inspection a map displaying the trends between magnetic and gravity intensities across the Tallaringa map sheet has been produced. Petrophysical density and magnetic susceptibility samples support the current domain boundaries based on prior TMI and Bouguer gravity map interpretations and may be applicable to two sub domains within the trough. Prior seismic traverses enabled confident depth to basement calculation to produce a forward models of two potential field traverses that satisfy the regional signals. Modelling has produced a hypothesis that the Tallaringa Trough is an intersection of a low susceptibility, high density body and the high susceptibility, low gravity western Mabel Creek Ridge.

Tables

Table 7: Euler Deconvolution Results for Potential Field model line 86AK-14 for magnetic and gravity contact structures

Table 8: Euler Deconvolution Results for Potential Field model line 86AK-14 for magnetic and gravity thin dike structures

Table 9: summary of overall geophysical attributes of domains of the Tallaringa map sheet.

Figures

Figure 1: Geological setting of the Tallaringa Trough. Includes surficial geology of the North Western Gawler Province, the boundaries of current major domains defined by geology or magnetic lineaments, drill holes used for potential field modelling and both seismic survey lines used to define the potential field traverse. The square denotes the Tallaringa 1:250,000 map sheet and is , projected in GDA94 MGA Zone 53.

Figure 2: Total Magnetic Intensity (TMI) map of the Tallaringa 1:250,000 map sheet projected in GDA94 MGA Zone 53. Includes the potential field model lines and drill hole positions with respect to magnetic anomalies.

Figure 3: Bouguer Gravity map of the Tallaringa 1:250,000 map sheet projected in GDA94 MGA Zone 53. Includes the potential field model lines and drill hole positions with respect to gravity anomalies.

Figure 4a: Seismic reflection and refraction survey 86 AK-12 across Tallaringa Trough. Two way time (msec) versus distance (m). Coloured lines indicate primary reflectors. Stratigraphic interpretation after Cockshell in Benbow (1993).

Figure 4b: Seismic reflection and refraction survey 86 AK-14 across Tallaringa Trough. Two way time (msec) versus distance (m). Coloured lines indicate primary reflectors. Stratigraphic interpretation after Cockshell in Benbow (1993).

Figure 5: Maps of gravity survey stations and aeromagnetic surveys conducted within the Tallaringa map sheet. Green, larger dots indicate gravity stations chosen by closest perpendicular distance to the potential field modelled lines. Both maps are projected in GDA94 MGA Zone 53.

Figure 6: Petrophysical statistical comparison of drill core from the western Gawler Province.

Figure 7: First Vertical Derivative (1VD) of the Tallaringa map sheet, projected in GDA94 MGA Zone 53.

Figure 8: Automatic Gain Control (AGC) of the 1VD overlaying the 1VD of the Tallaringa map sheet, projected in GDA94 MGA Zone 53. Note the discordance where high detailed anomalies in 1VD have been smoothed by AGC to “equalise” with lower frequency anomalies of the study area.

Figure 9a: Tilt derivative of the Reduced To Poles (RTP) map with automatic contouring in Oasis Montaj where the tilt derivative = 0.
Figure 9b: The Reduced to Poles (RTP) overlain with the above contour lines to compare the detected edges of continuous magnetic bodies with a map typically used to delineate edges by visual recognition.

Figure 10: Euler Deconvolution generated in Matlab from the TMI of the 86AK-14 traverse demonstrating that depth to source estimates of the technique are related to the structural index. There is approximately 1km of difference between the shapes that can generate the TMI field within the 31 - 34 km range.

Figure 11: Extended Euler Deconvolution results for profile 86AK-12 for a 1 km window. Top displays detected the positions for (SI = 0) magnetic contacts, their depth, angle of dip and susceptibility contrast. Bottom displays detected positions for SI = 1 (dike like structures), their dip angle and susceptibility x thickness.

Figure 12: Extended Euler Deconvolution results for profile 86AK-12 for a 2 km window. Top displays detected the positions for (SI = 0) magnetic contacts, their depth, angle of dip and susceptibility contrast. Bottom displays detected positions for SI = 1 (dike like structures), their dip angle and susceptibility x thickness.

Figure 13: Extended Euler Deconvolution results for profile 86AK-12 for a 5 km window. Top displays detected the positions for (SI = 0) magnetic contacts, their depth, angle of dip and susceptibility contrast. Bottom displays detected positions for SI = 1 (dike like structures), their dip angle and susceptibility x thickness.

Figure 14: Extended Euler Deconvolution results for profile 86AK-12 for a 10 km window. Top displays detected the positions for (SI = 0) magnetic contacts, their depth, angle of dip and susceptibility contrast. Bottom displays detected positions for SI = 1 (dike like structures), their dip angle and susceptibility x thickness.

Figure 15: Extended Euler Deconvolution results for profile 86AK-14 for a 1 km window. Top displays detected the positions for (SI = 0) magnetic contacts, their depth, angle of dip and susceptibility contrast. Bottom displays detected positions for SI = 1 (dike like structures), their dip angle and susceptibility x thickness.

Figure 16: Extended Euler Deconvolution results for profile 86AK-14 for a 2 km window. Top displays detected the positions for (SI = 0) magnetic contacts, their depth, angle of dip and susceptibility contrast. Bottom displays detected positions for SI = 1 (dike like structures), their dip angle and susceptibility x thickness.

Figure 17: Extended Euler Deconvolution results for profile 86AK-14 for a 5 km window. Top displays detected the positions for (SI = 0) magnetic contacts, their depth, angle of dip and susceptibility contrast. Bottom displays detected positions for SI = 1 (dike like structures), their dip angle and susceptibility x thickness.

Figure 18: Extended Euler Deconvolution results for profile 86AK-14 for a 10 km window. Top displays detected the positions for (SI = 0) magnetic contacts, their depth, angle of dip and susceptibility contrast. Bottom displays detected positions for SI = 1 (dike like structures), their dip angle and susceptibility x thickness.

Figure 19: Geophysical interpretation of magnetic bodies over the Bouguer Gravity map of the Tallaringa mapsheet, projected in GDA94 MGA Zone 53. Bodies are coloured by magnetic amplitude to display the changing association of magnetism with gravity between domains.

Figure 20: Geophysical interpretation of the Tallaringa map sheet, projected in GDA94 MGA Zone 53.

References

Barclay, C. J. (1975). Open File Envelope 2613: Exploration License 175 Relinquishment Report August 1975, Shell Development (Australia) Pty Ltd**:** 46.

Benbow, M. C. (1986). Sheet SH 53-5 Tallaringa 1:250 000. S.A. Geological Atlas Series. Adelaide, Department of Mines and Energy.

Benbow, M. C. (1993). Tallaringa 1:250 000 Geological Series - Explanatory Notes. J. Selby. Adelaide, Geological Survey South Australia.

Betts, P. G. (2000). "Tectonic Evolution of the Cooper Pedy Ridge and Mabel Creek Ridge from Potential Field interpretation." Australian Crustal Research Centre(83): 1 - 24.

Betts, P. G., R. K. Valenta, et al. (2003). "Evolution of the Mount Woods Inlier, northern Gawler Craton, South Australia: an intergrated structural and aeromagnetic analysis." Tectonophysics(366): 83 - 111.

Daly, S. J., C. M. Fanning, et al. (1998). "Tectonic evolution and exploration of the Gawler Craton, South Australia." Journal of Australian Geology & Geophysics **19**(3): 145-168.

Direen, N. G., A. G. Cadd, et al. (2005). "Architecture of Proterozoic shear zones in the Christie Domain, western Gawler Craton, Australia: Geophysical appraisal of a poorly exposed orogenic terrane." Precambrian Research(142): 28-44.

Dreverman, P. C. and G. C. Reveleigh (1980). Envelope 3057: Completion Exploration Report on EL 288 Indooroopilly, S.A., Australian Development Limited; Noblex N.L.**:** 53.

Drexel, J. F., W. V. Priess, et al. (1993). The geology of South Australia Volume 1 The Precambian. Bulletin 54. **1:** 249.

Finlayson, B. (1979). Report Book 79/90 A Geophysical interpretation with depths to magnetic basement - Tallaringa, Giles, Murloocoppie 1:250 000 sheets Adelaide, Department of Mines and Energy South Australia**:** 1 - 35.

Fraser, G. L. and P. Lyons (2006). "Timing of Mesoproterozoic tectonic activity in the northwestern Gawler Craton constrained by Ar^{40}/Ar^{39} geochronology." Precambrian Research(151): 160-184.

Gatehouse, C. G. (1979). Well Completion Report Wilkinson No. 1. Adelaide, Department of Mines and Energy South Australia**:** 1 - 158.

Gatehouse, C. G., J. K. Warren, et al. (2002). Open File Envelope No. 9597, EL 2569 Wilkinson Annual and Final Reports for the Period 4/1/99 To 3/1/2002. EL 2569. Adelaide, Primary Industries and Resources SA**:** 791.

Giles, D., P. G. Betts, et al. (2004). "1.8 - 1.5 Ga links between the North and South Australian Cratons and the Early-Middle Proterozoic configuration of Australia." Tectonophysics(380): 27-41.

Hand, M., A. Reid, et al. (2007). "Tectonic Framework and Evolution of the Gawler Craton, South Australia." Economic Geology **102**: 18.

Heath, P., T. Dhu, et al. (2009). "Geophysical modelling of the Gawler Province SA - interpreting geophysics with geology." Exploration Geophysics **40**(4): 342-351.

Jessell, M. and R. K. Valenta (1996). "Structural geophysics: integrated structural and geophysical modelling." Structural Geology and Personal Computers: 303-324.

Kay, B. D. and D. F. Robson (1981). Open File Envelope No. 3887. Adelaide, PIRSA**:** 106.

Lahti, I. and T. Karenen (2010). Tilt Serivative multiscale edges of magnetic data. The Leading Edge**:** 9.

Milton, B. E. (1974). Reconnaissance Seismic Exploration - Southwest Ackaringa Basin, South Australia, 1974. Adelaide, Department of Mines South Australia**:** 1 - 12.

Morris, B. J., P. W. Hill, et al. (1994). Report Book 94/19 Barton Bedrock Drilling Project 1993. Adelaide, Department of Mines and Energy, South Australia. **1:** 734.

Parker, A. J. (1987). Ooldea 3: Well-completion report and tectonic modelling. Adelaide, South Australia: Department of Mines and Energy**:** 58.

Payne, J. L., K. M. Barovich, et al. (2006). "Provenance of metasedimentary rocks in the northern Gawler Craton, Australia: Implications for Palaeoproterozoic reconstructions." Precambrian Research(128): 275 - 291.

Payne, J. L., M. Hand, et al. (2008). "Temporal constraints on the timing of high grade metamorphism in the northern Gawler Craton: implications for assembly of the Australian Proterozoic." Australian Journal of Earth Sciences(55): 623-640.

Rankin, L. R., A. R. Martin, et al. (1989). "Early Proterozoic history of the Karari Fault Zone, northwest Gawler Craton, South Australia." Australian Journal of Earth Sciences(36): 123 - 133.

Reid, A. B., J. M. Allsop, et al. (1990). "Magnetic interpretation in the dimensions using Euler deconvolution." Geophysics **55**(1): 80-91.

Swain, G. M., M. Hand, et al. (2005). "Age Constraints on terrane-scale shear zones in the Gawler Craton, southern Australia." Precambrian Research **139**: 164-180.

Teasdale, J. (1997). Methods for understanding poorly exposed terranes: the interpretive geology and tectonothermal evolution of the western Gawler Craton. PhD Thesis, University of Adelaide.

Thompson, D. T. (1982). "EULDPH: A new technique for making computer-assisted depth estimates from magnetic data." Geophysics **47**(1): 31-37.

Verduzco, B., J. D. Fairhead, et al. (2004). New Insights into magnetic derivatives for structural mapping. The Leading Edge**:** 4.

Tables

Event	Age (Ma)	Region
Kimban Orogeny	1730 - 1690	Entire Craton
Ooldean Event	1650	Ooldea/Moondrah
Kararan	1570 – 1545	Northern and Western
Karari Reactivation	>1450	Northern and Western

Table 1: Edited list of dated tectonic events specific to the western Gawler Province. (KFZ – Karari Fault Zone) (Payne et al. 2008)

Drill hole	Latitude (dec. deg)	Longitude (dec. deg)	Domain	Interval (m)	Lithology	Mean M.S. (SI x 10^{-5})	Mean Density (kgm^{-3})
OBD 1	-29.31	132.56	Nawa	116 – 139.8	Granite; tonalite; gneiss; gabbro; basalt; pyroxenite; peridotite; komatiite.	1809 +/- 1214	2827 +/- 84
OBD 3	-29.46	132.30	Nawa	132 – 217.8	Granite, partly gneissic and chloritic	248 +/- 250	2674 +/- 42
OBD 12	-29.60	132.25	Nawa	464 - 472	Pink granite, gneiss	459 +/- 466	2740 +/- 85
LBR 20	-30.32	132.62	Christie	52 - 55	Bi-amp-feld	11 +/- 3	
LBR 21	-30.31	132.62	Christie	74 – 75	bi-feld minor qtz, py, monzodiorite	535 +/- 0	
LBR 40	-30.25	132.71	Christie	78 – 81	plag-qtz-k-feld, granite gneiss + garnet	104 +/- 58	
NNL IL1 DDH2	-29.63	133.07	Christie	46 – 206	Pyroxene granulite of qtz/parthite/hyperthene	415 +/- 424	2684 +/- 309
NNL IL2 DDH1	-29.63	133.07	Christie	36 – 190	Pyroxene granulite of qtz/parthite/hyperthene	698 +/- 1204	3095 +/- 675
Ooldea 1	-30.46	131.63	Moondrah	287 - 295	Pink mg adamellite gneiss	0	2583 +/- 47
Ooldea 2	-30.58	131.75	Moondrah	35 - 165	Mg-cg banded qtz-feld-mt-gt-(px-amph-bi)gneiss	19626 +/- 17995	3111 +/- 197
Ooldea 3	-30.62	131.91	Moondrah	101 - 370	Mass-banded mg qtz-mt gneiss (BIF), mylonite/pegmatite	4902 +/- 11697	2785 +/- 907
Piglet 1	-29.84	132.53	Tallaringa Trough	185 - 685	Mudstone/Sandstone/Halite	3 +/- 1	2398 +/- 125
Wilkinson 1	-29.94	132.51	Tallaringa Trough	210 - 700	Mudstone/Sandstone/Halite	0	2429 +/- 117

Amp/amph, amphibole; bi, biotite; fsp, feldspar; gt, garnet; k feld, potassium feldspar; mt, magnetite; plag, plagioclase; px, pyroxene; py, pyrite; qtz, quartz; dec. deg, decimal degrees

Table 2: Sample drill holes to basement, intervals and basement lithologies. Table summary of the drill holes and basement petrophysics sourced from the PIRSA core library, taken from open file company reports or supplied by Dr Graham Baines.

Magnetic Amplitude	**Magnetic Texture**	**Magnetic Wavelength**	**Gravity Amplitude**
Very High - M1	Convoluted – T1	Very Short –W1	Very High – G1
High - M2	Sinuous - T2	Short –W2	High – G2
Average – M3	Mottled - T3	Average – W3	Average – G3
Low – M4	Linear/Banded – T4	Long – W4	Long – G4
Very Low – M5	Diffuse – T5	Very Long – W5	Very Low – G5

Table 3: the four by fields assigned to describe a magnetic subdomain. The numeric values of each field combines into a 4 digit number that is recorded as the Geophysical ID number for later manipulation of maps by characteristics.

Source Shape	**Gravity SI**	**Magnetic SI**
Sphere	2	3
Horizontal cylinder	1	2
Fault / Thin Dike	0	1
Contact	-1	0

Table 4: Fitzgerald et al, (2004) table of SI: structural indexes for gravity and magnetic potential field analysis by Euler Deconvolution. Numbers substitute for *N* in equation 1. An index directly affects the estimated distance to the source from the measured field.

Table 5: Euler Deconvolution results for Potential Field model line 86AK-12 for magnetic and gravity contact structures

Gravity				
Window Size	**Xconv**	**Zconv**	**Dip**	**Count**
10x1	21.285	0.465333	164.2633	3
	22.629	1.918333	27.31667	3
	53.749	1.446	88.52	1
	57.02933	1.477333	114.6833	3
10x2	31.5595	1.66	111.02	2
	48.704	3.104	30.42	1
	56.235	0.919	104.235	2
	58.072	1.661	140.76	1

Magnetic								
Window Size	**Xconv**	**Zconv**	**Xext**	**Zext**	**Dip**	**Dip S.D.**	**Susc**	**Count**
10x1	1.90900	0.22950	1.91100	0.24550	153.56000	-0.00101	8.14587	2
	3.07733	0.23350	3.05967	0.22350	119.84500	0.00087	24.59288	6
	4.30800	0.40900	4.35300	0.40300	91.50000	-0.00090	0.00000	1
	5.71900	0.22050	5.68300	0.23500	27.12000	0.00154	1.35765	2
	7.17000	0.23100	7.17400	0.27600	119.02000	-0.00115	0.00000	1
	8.33100	0.28117	8.33967	0.27283	56.94833	0.00227	22.92182	6
	11.25183	0.13167	11.23117	0.14017	56.29833	-0.00123	26.93209	6
	12.60940	0.23440	12.59260	0.22320	120.90200	0.00103	28.20479	5
	13.89050	0.25125	13.89650	0.23100	110.47750	-0.00213	67.52234	4
	15.11367	0.18550	15.12733	0.19433	109.47333	0.00280	54.36927	6
	15.60300	0.22100	15.61200	0.19000	2.88000	-0.02308	0.00000	1
	15.58500	0.22500	15.60900	0.18300	179.59000	0.16099	0.00000	1
	16.30000	0.30800	16.32700	0.26700	99.41000	-0.00122	0.00000	1
	17.65400	1.01700	17.63000	0.97400	7.13000	0.01295	0.00000	1
	34.03300	1.05100	33.98600	1.01400	87.93000	-0.00045	0.00000	1
	37.85240	0.19820	37.84750	0.19550	111.99500	0.00014	36.34406	10
	41.7397	0.2673	41.7353	0.2654	88.0755	-	59.1093	9

	8	3	3	4	6	0.00053	3	
	51.36227	0.25591	51.37591	0.25927	104.77909	-0.00482	65.05383	11
	58.75780	0.34800	58.77400	0.33360	106.89600	0.00454	58.53411	5
	65.78920	0.11980	65.78350	0.12350	101.26800	-0.00007	24.68181	10
	77.31225	0.13088	77.30588	0.12325	87.97563	-0.00005	64.30817	16
	80.03450	0.10750	80.01350	0.10975	125.94000	-0.00003	14.71556	4
	84.07100	0.14688	84.09313	0.12713	86.02875	-0.00003	80.29211	8
10x2	2.01300	0.19300	1.95600	0.11900	144.96000	-0.00077	0.00000	1
	2.81450	0.10100	2.80950	0.16600	77.50000	0.00084	27.42160	2
	4.39000	0.38375	4.41750	0.36350	86.23000	-0.00286	66.03508	4
	8.38227	0.23618	8.35900	0.24945	58.28455	0.00343	23.42827	11
	11.99550	0.06300	11.96300	0.06050	76.96500	-0.00093	28.91717	4
	15.41000	0.16100	15.31600	0.07800	127.16000	0.00152	0.00000	1
	17.14671	0.51200	17.13171	0.51043	98.36000	-0.00813	57.34418	7
	22.42100	1.29700	22.41900	1.22800	162.05000	0.00849	0.00000	1
	24.24817	1.29800	24.26183	1.30783	48.27167	-0.00454	27.50554	6
	30.90600	0.84600	30.87860	0.82400	102.97200	0.00222	70.41582	5
	34.55600	0.83575	34.55738	0.84700	120.21625	-0.00083	39.34093	8
	37.57600	0.24275	37.51025	0.20925	132.35500	0.00052	16.45577	4
	38.19800	0.19140	38.18800	0.22140	53.27000	-0.00136	34.23606	5
	41.40378	0.21000	41.40233	0.24111	101.58222	0.01455	33.25628	9
	42.46367	0.33900	42.44750	0.34533	47.05167	-0.00084	11.19378	6
	51.07700	0.28600	51.12386	0.24986	124.00143	0.00104	31.09886	7
	51.71775	0.15650	51.70100	0.21775	24.02250	-0.00161	13.57253	4
	58.30150	0.34450	58.28450	0.31650	138.69000	0.01598	37.99794	6
	61.05667	0.21927	61.06427	0.22387	61.58133	-0.01554	39.82301	15
	70.37500	0.00600	70.29900	0.05500	24.21000	0.00007	0.00000	1
	71.15900	0.18300	71.06700	0.17800	169.42000	-0.00030	0.00000	1
	71.36767	0.06800	71.35033	0.08800	31.48000	0.00033	46.61822	3
	78.0367	0.0695	78.0917	0.0772	114.115	-	67.6206	7

	1	7	1	9	71	0.00030	0	
	81.78600	0.08300	81.70400	0.08600	82.71000	0.00005	0.00000	1
	84.03400	0.13500	84.03450	0.08750	156.52500	0.00019	13.45624	2
10x5	4.70114	0.07614	4.73514	0.05829	90.91000	-0.00141	50.22975	7
	8.37813	0.15271	8.36426	0.12648	71.91355	0.00277	33.32867	31
	14.53064	0.11529	14.54700	0.04614	75.34214	-0.00239	45.08956	14
	20.99517	1.20250	20.96667	1.24817	114.92000	0.00589	47.06506	6
	24.83600	0.93586	24.89829	1.05414	74.35571	-0.00533	62.99059	7
	42.10883	0.19470	42.10378	0.20370	98.94304	0.00096	63.25800	23
	47.49467	1.79567	47.58833	1.87700	1.61333	0.11380	1.38399	3
	47.60100	1.66100	47.69400	1.51200	176.39000	-0.00929	0.00000	1
	50.76444	0.46233	50.78967	0.34300	110.41889	0.00090	45.53544	9
	53.09500	0.08600	52.88900	0.20900	88.43000	-0.00088	0.00000	1
	58.56352	0.16313	58.52352	0.13904	138.39609	0.00929	30.50697	23
	62.94056	0.23440	62.94532	0.24260	73.50680	-0.04471	55.03400	25
	77.57375	0.06350	77.61300	0.03075	58.23500	0.00005	28.17551	4
	78.21767	0.09833	78.12833	0.03267	127.32667	-0.00004	15.76377	3
	83.31100	0.09450	83.17550	0.05200	98.07500	0.00009	1.18087	2
10x10	6.85740	0.26640	6.91760	0.06920	45.27800	10.68346	0.00176	5
	7.30400	0.00900	7.28900	0.06100	171.70000	0.00000	-0.00942	1
	8.20833	0.31389	8.19589	0.04000	58.40556	33.20288	0.00317	9
	10.30700	0.47200	9.86600	0.00400	158.12000	0.00000	-0.00087	1
	10.13500	0.35067	10.09433	0.05767	46.71000	13.56559	0.00173	3
	14.59125	0.31300	14.63963	0.04250	130.74125	45.66268	-0.00605	8
	18.66767	0.39433	18.96967	0.20967	108.52333	54.00301	0.00716	3
	24.03218	0.22700	24.12376	0.30600	63.07353	45.27971	-0.00484	17
	37.39525	0.23825	37.10550	0.08300	75.99750	57.73476	-0.00064	4
	41.74375	0.29444	41.69963	0.05513	55.86750	22.24049	-0.00085	16
	50.61480	0.26460	50.61180	0.04380	75.58800	3.42511	0.00059	5

	58.12133	0.18133	58.11517	0.06900	133.04500	26.09070	0.00290	6
	58.70900	0.16400	58.68100	0.01900	4.43000	0.00000	-0.02416	1
	58.67050	0.07350	58.74338	0.01813	164.31000	7.09474	0.00759	8
	60.07965	0.26890	60.07665	0.13115	52.75800	33.91014	-0.00393	20
	78.86300	0.22350	78.85250	0.07200	99.37500	11.92889	0.00007	2

Table 6: Euler Deconvolution results for Potential Field model line 86AK-12 for magnetic and gravity thin dike structures

Gravity				
Window Size	**Xconv**	**Zconv**	**Dip**	**Count**
10x1	42.251	6.858	144.71	1

Magnetic								
Window Size	**Xconv**	**Zconv**	**Xext**	**Zext**	**Dip**	**Dip S.D.**	**Susc*thicknes**	**Count**
10x1	37.46700	0.37400	37.46700	0.46000	83.54000	0.00000	0.00019	1
	79.97800	0.37200	80.04500	0.43500	39.26000	0.00000	-0.00003	1
10x2	1.88600	0.21700	1.73000	0.02800	175.15000	0.00000	0.00217	1
	4.93700	0.89500	5.00100	0.87600	42.55000	0.00000	-0.00347	1
	31.54133	1.31833	31.56500	1.15633	42.81333	4.74978	0.00099	3
	34.88700	1.43200	34.88700	1.56500	55.18000	0.00000	-0.00150	1
	37.50200	0.59800	37.40100	0.71900	44.13000	0.00000	0.00083	1
	41.65067	0.65333	41.62300	0.51300	37.06000	4.86519	0.00152	3
	51.23283	0.66750	51.27783	0.58100	51.81833	13.44241	0.00083	6
	66.03950	0.36400	66.20850	0.23900	91.22000	123.13557	0.00080	2
	71.18467	0.06133	71.16133	0.06367	71.64667	86.88161	0.00002	3
10x5	16.83400	0.54600	17.08400	0.14500	23.31000	0.00000	-0.01150	1
	41.87629	0.59971	41.58243	0.17686	54.59000	14.52593	0.00208	7
	51.20754	0.54223	51.27262	0.22338	70.94846	16.71322	0.00090	13
	58.52233	0.88433	58.19800	1.10433	59.45000	6.52635	0.00946	3
	76.93000	0.02300	77.37900	0.00600	177.93000	0.00000	-0.00170	1
	80.94000	0.07800	80.50900	0.00200	100.48000	0.00000	-0.00007	1
10x10	51.53200	0.05400	50.92800	0.19100	33.14000	0.00000	0.00542	1
	58.75308	0.77120	58.18063	0.13930	80.08300	12.83788	0.00760	22

Table 7: Euler Deconvolution Results for Potential Field model line 86AK-14 for magnetic and gravity contact structures

Gravity

Window Size	Xconv	Zconv	Dip	Count
10x1	9.08	0.62	151.49	1
	36.44	0.95	158.21	2
	50.79	1.42	104.76	4

Magnetic

Window Size	Xconv	Zconv	Xext	Zext	Dip	Dip S.D.	Susc	Count
10x1	0.74700	0.31700	0.78200	0.34900	43.33000	0.00000	-0.00058	1
	2.34767	0.27433	2.33367	0.27967	159.00333	1.85745	-0.00097	3
	3.31375	0.24250	3.29000	0.26025	85.02000	7.11695	0.00065	4
	3.51700	0.18700	3.55300	0.20200	137.24000	0.00000	0.00073	1
	6.38350	0.18550	6.38650	0.22300	58.39500	7.51655	-0.00075	2
	8.05000	0.65800	8.05700	0.67600	29.11000	3.52139	0.00183	2
	15.85700	0.39100	15.83800	0.42400	71.73000	0.00000	0.00118	1
	18.84457	0.63786	18.85171	0.65586	40.29429	6.39621	-0.00532	7
	29.66840	0.55000	29.64740	0.55060	34.46400	2.79899	-0.00031	5
	34.94300	0.80771	34.95329	0.81543	78.20429	7.86886	-0.00064	7
	43.61150	0.47300	43.57850	0.49500	80.37000	7.41048	0.00044	2
	45.99450	0.88650	45.97650	0.90100	103.97000	0.22627	-0.00065	2
	47.58800	1.48500	47.58400	1.46100	169.77000	0.00000	-0.00513	1
	49.87400	0.91300	49.87500	0.92300	76.91000	0.00000	0.00119	1
	50.91533	0.56867	50.92700	0.55367	164.11667	5.48046	0.00482	3
	52.11400	0.75700	52.10200	0.75550	56.84500	2.12839	-0.00114	2
	57.96600	0.37167	57.94800	0.38100	127.55333	4.22827	0.00163	3
	58.95050	0.35000	58.96150	0.37950	45.19000	23.97092	-0.00282	2
	64.73600	0.18500	64.76000	0.16000	127.51000	0.00000	-0.00079	1
	66.52500	0.21500	66.49400	0.19300	135.84000	0.00000	0.00149	1
	66.83833	0.08383	66.83283	0.09217	37.59833	10.12026	-0.00161	6
	68.31200	0.17400	68.26700	0.19900	155.64000	0.00000	-0.00355	1
	71.79900	0.05900	71.79880	0.09660	73.09400	17.77147	0.00089	5
	74.34388	0.01713	74.35238	0.01675	72.60875	31.72545	-0.00039	8
	75.74000	0.04200	75.73900	0.00000	107.96000	0.00000	0.00008	1
	75.76000	0.02300	75.80100	0.00100	14.91000	0.00000	0.00005	1
	75.81600	0.00600	75.84200	0.00300	175.06000	0.00000	-0.00110	1
10x2	1.92400	0.48833	1.92267	0.45967	128.24333	41.16981	-0.00115	3
	3.49254	0.23015	3.48131	0.19677	117.54769	25.92165	0.00125	13
	6.18513	0.06275	6.24575	0.05738	44.00625	10.67801	-0.00048	8
	6.61700	0.12100	6.52100	0.19500	80.19000	0.00000	-0.00077	1
	8.28650	0.48300	8.35100	0.56000	50.21000	5.60029	0.00128	2
	12.59625	0.10300	12.63900	0.05975	129.33750	26.63486	-0.00054	4
	13.16300	0.02600	13.25300	0.04900	26.46000	0.00000	0.00073	1
	13.79800	0.07567	13.77167	0.05267	137.17500	31.62609	0.00091	6

	13.94500	0.11200	14.02600	0.02700	1.79000	0.00000	-0.00759	1
	16.14300	0.13040	16.14680	0.11480	116.23400	16.96485	0.00056	5
	18.80120	0.55000	18.82220	0.60060	37.87400	6.02358	-0.00575	5
	20.55533	0.84717	20.54500	0.86333	123.24667	2.74974	-0.00214	6
	24.21867	0.39900	24.25800	0.36600	71.74333	0.83764	0.00035	3
	29.77493	0.63213	29.77700	0.62587	39.07533	4.94482	-0.00032	15
	35.05664	0.81455	35.03082	0.80027	82.67364	6.73461	-0.00064	11
	43.44350	0.69750	43.39088	0.74638	67.37375	26.69406	0.00070	8
	45.09300	0.52000	45.06800	0.60300	43.84000	0.00000	-0.00090	1
	50.06400	0.77100	50.11500	0.80100	87.47000	0.00000	0.00125	1
	51.48800	0.65500	51.41200	0.69500	22.85000	0.00000	-0.00327	1
	57.86717	0.34200	57.87408	0.35825	121.16417	9.77107	0.00133	12
	58.72333	0.26333	58.70300	0.34133	29.78333	5.70075	-0.00403	3
	58.92160	0.40180	58.89560	0.36620	43.80400	2.36909	-0.00234	5
	62.89100	0.02800	62.84700	0.06300	31.85000	0.00000	0.00049	1
	62.95400	0.06600	62.88000	0.08100	178.96000	0.00000	-0.01367	1
	63.87400	0.03500	63.80000	0.01400	85.50000	0.00000	0.00079	1
	66.57750	0.09600	66.62300	0.04650	154.77000	18.62402	0.00360	4
	66.80000	0.07025	66.84625	0.08650	16.53500	28.57811	-0.06802	4
	68.48100	0.29500	68.53100	0.21000	11.47000	0.00000	0.01319	1
	69.25000	0.05167	69.20950	0.01833	114.22333	27.25420	0.00296	6
	69.86100	0.04600	69.95400	0.00300	171.71000	0.00000	-0.00393	1
	72.37233	0.08300	72.42333	0.04333	123.52333	24.40870	0.00079	3
	74.42100	0.02850	74.43200	0.01550	101.95500	36.29291	-0.00045	4
	78.09400	0.09833	78.12500	0.01567	149.28333	13.22687	0.00151	3
	78.36725	0.01525	78.35850	0.01275	46.17250	42.85293	-0.00344	4
10x5	3.42400	0.08800	3.53150	0.01800	54.67500	4.57498	0.00066	2
	4.60125	0.19000	4.63025	0.03175	148.15500	9.62375	0.00164	4
	4.99600	0.03800	5.15500	0.05500	21.59000	0.00000	-0.00245	1
	6.87300	0.27133	6.79533	0.08767	129.31667	7.23217	-0.00114	3
	7.24200	0.00900	7.32200	0.00700	175.72000	0.00000	-0.00908	1
	7.60200	0.19000	7.71700	0.00000	60.38000	0.00000	0.00016	1
	8.21767	0.19967	8.22200	0.05267	162.43333	12.43601	-0.00393	3
	8.31100	0.08600	8.50100	0.08500	4.52000	0.00000	0.00982	1
	9.93747	0.18247	9.88767	0.10493	113.54800	32.69857	0.00095	15
	10.53650	0.09500	10.64000	0.03850	16.51500	14.21992	-0.00264	2
	12.61900	0.11750	12.53200	0.00700	143.70500	10.54296	0.00071	2
	15.09160	0.12720	15.14700	0.02820	32.57800	10.86747	0.00094	5
	16.22700	0.01200	16.46600	0.09200	57.96000	0.00000	0.00106	1
	18.05917	0.30417	17.91567	0.18217	143.23833	18.37953	0.01548	6
	18.60932	0.20477	18.69032	0.27586	34.11364	14.91429	-0.00824	22
	20.89500	0.62400	21.06600	0.78700	159.50000	0.00000	-0.00497	1
	24.38133	0.44167	24.45767	0.35717	89.99833	1.87339	0.00030	6
	29.98533	0.63392	29.93600	0.49317	51.92417	4.50300	-0.00020	12
	34.89658	0.54200	34.96827	0.57930	74.20636	9.38623	-0.00055	33
	43.31242	0.50783	43.35217	0.54875	59.55583	8.00912	0.00064	12
	50.63660	0.30000	50.77120	0.20960	146.14600	39.79809	0.00374	5
	50.95700	0.03750	51.19150	0.15900	14.26000	2.58801	-0.00443	2
	58.24781	0.24958	58.20596	0.17804	134.35885	33.04296	0.02847	26
	58.77163	0.14126	58.84353	0.17642	34.21842	25.71702	-0.00686	19
	64.23300	0.12100	64.20950	0.05300	38.85000	6.75994	0.00088	2
	67.83250	0.24100	67.96500	0.09000	12.19000	0.33941	0.00911	2
	68.05300	0.14750	68.25550	0.07150	44.67000	13.66130	0.00209	2

	69.23100	0.00800	68.98500	0.00200	172.14000	0.00000	-0.00393	1
	69.58514	0.16486	69.54071	0.02757	68.19714	41.28408	0.00231	7
	74.04800	0.13000	73.99620	0.05420	92.38200	59.20924	-0.00534	5
10x10	10.30600	0.35650	10.53000	0.02900	122.51500	31.62889	0.00041	2
	12.97767	0.28400	12.84767	0.08650	78.00667	21.32622	0.00108	6
	16.82500	0.37850	17.12100	0.18100	145.94500	19.62221	0.00463	2
	17.36300	0.11100	17.59700	0.24600	173.80000	0.00000	0.02497	1
	17.89569	0.23877	17.88762	0.13246	20.88538	16.42669	-0.01097	13
	17.88800	0.21450	18.11550	0.01650	169.35000	4.42649	0.00661	2
	18.97124	0.22962	18.94405	0.08476	79.03143	31.97446	-0.00185	42
	34.73166	0.49738	34.86400	0.55528	88.57641	7.74702	-0.00051	64
	47.12533	0.43033	46.74100	0.14067	167.80000	12.03538	-0.00455	3
	49.37038	0.31275	49.24538	0.06813	120.22250	30.61895	0.00111	8
	50.32800	0.28300	49.86600	0.02200	12.55000	0.00000	-0.00156	1
	58.87900	0.14000	59.05500	0.00200	165.63000	0.00000	0.00159	1
	61.31625	0.38375	61.07575	0.07000	56.22500	19.05254	-0.00249	4
	68.72167	0.42883	68.60067	0.06700	63.88500	34.27977	0.00301	6
	69.85500	0.25350	69.83550	0.02300	29.94500	17.93930	-0.00267	2
	70.07900	0.35800	70.18600	0.01000	162.70000	0.00000	0.00238	1
	70.88200	0.43700	71.32700	0.12800	79.22000	0.00000	-0.00232	1

Table 8: Euler Deconvolution Results for Potential Field model line 86AK-14 for magnetic and gravity thin dike structures

Gravity

Window Size	Xconv	Zconv	Dip	Count
10x1	21.7305	1.1645	53.99	2
10x2	21.7145	0.614	55.635	2
10x5	11.9195	2.9685	71.33	2
	43.18	2.922	49.89	1

Magnetic								
Window Size	**Xconv**	**Zconv**	**Xext**	**Zext**	**Dip**	**Dip S.D.**	**Susc**	**Count**
10x1	50.75000	1.02000	50.66600	1.04100	47.44000	0.00000	0.00323	1
	64.04600	0.43900	64.03600	0.34900	51.36000	0.00000	0.00078	1
10x2	1.99400	0.99600	1.98500	0.86500	58.40000	0.00000	-0.00120	1
	11.24700	0.43600	11.32800	0.24500	62.65000	0.00000	0.00064	1
	14.96700	0.20300	14.87000	0.03400	179.28000	0.00000	0.03729	1
	50.75333	1.15800	50.62133	1.12722	54.64778	1.89062	0.00344	9
	78.02800	0.21000	77.90900	0.07400	29.64000	0.00000	0.00076	1
10x5	6.78100	0.81400	7.07400	0.56150	57.45000	7.39634	-0.00224	2
	29.41150	0.35850	29.32450	0.05050	94.57000	120.19401	0.03113	2
	50.72667	1.29600	50.61967	0.83133	55.35333	11.92007	0.00486	3
	76.69900	0.28800	76.59500	0.14600	1.22000	0.00000	0.11723	1
	77.26600	0.09200	77.39200	0.00500	18.91000	0.00000	0.00745	1
10x10	20.37300	0.61500	21.18500	0.08500	73.50000	0.00000	-0.00380	1
	44.14450	1.03900	44.06950	0.09250	30.71000	0.56569	0.00594	2
	58.69125	0.95425	58.08225	0.11475	83.95250	23.38515	0.00411	4

Domain	Gravity Amplitude	Magnetic Amplitude	Magnetic Frequency	Wavelength
Western Mabel Creek	Low	Moderate - high	Moderate - high	Moderate to shallow
Central Nawa	Low	Moderate	High	Shallow
Moondrah Gneiss	High	Moderate - low	Moderate	Moderate - deep
Western Tallaringa Trough	Low	Moderate - high	Moderate – high	Moderate - deep
Central Tallaringa Trough	High	Low	Low	Moderate
South Eastern Tallaringa Trough	Low	Moderate – low	Moderate	Moderate
North Eastern Tallaringa Trough	Low	Moderate - low	Moderate	Moderate

Table 9: summary of overall geophysical attributes of domains of the Tallaringa map sheet.

Figures

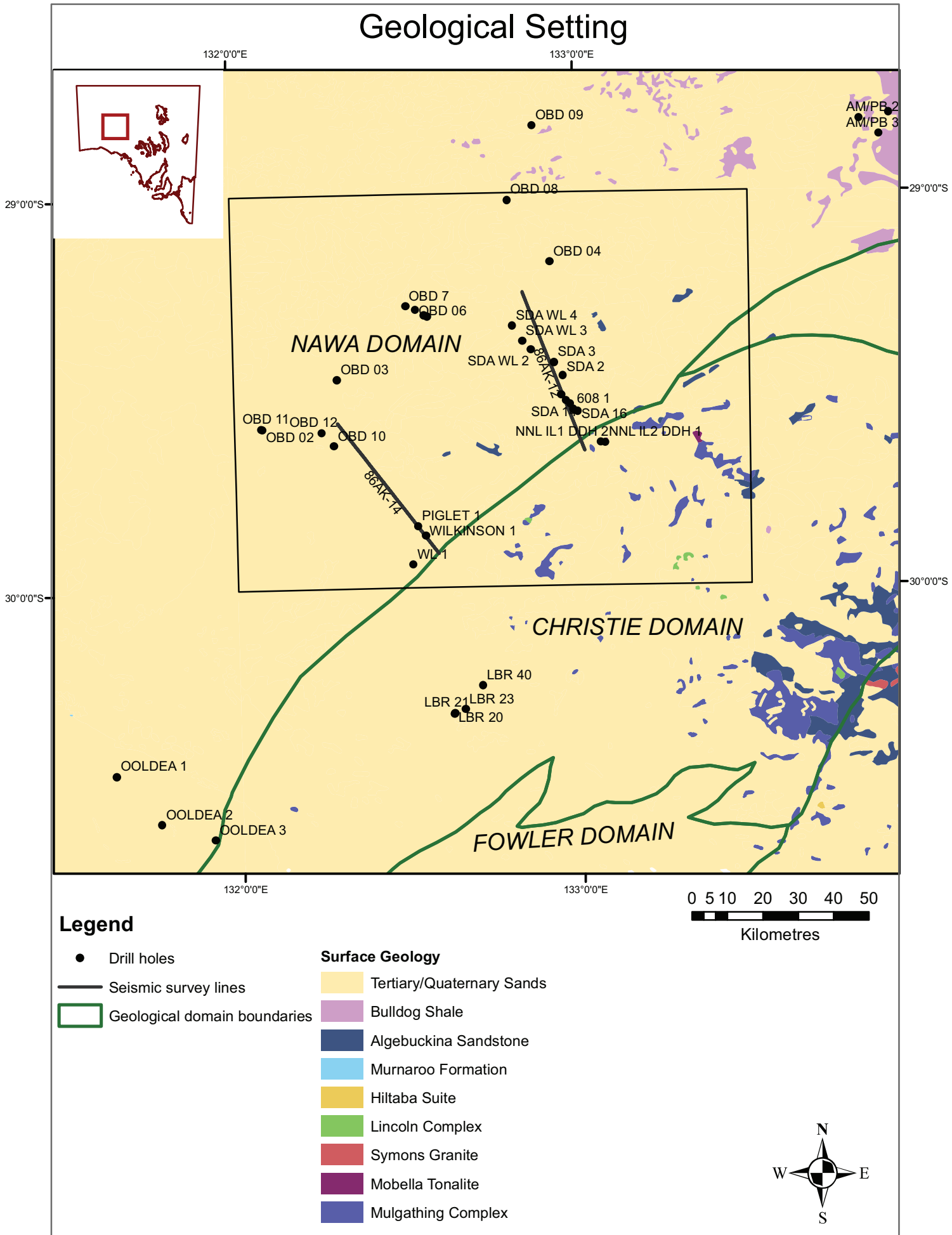

Figure 1: Geological setting of the Tallaringa Trough. Includes surficial geology of the North Western Gawler Province, the boundaries of current major domains defined by geology or magnetic lineaments, drill holes used for potential field modelling and both seismic survey lines used to define the potential field traverse. The square denotes the Tallaringa 1:250,000 map sheet and is , projected in GDA94 MGA Zone 53.

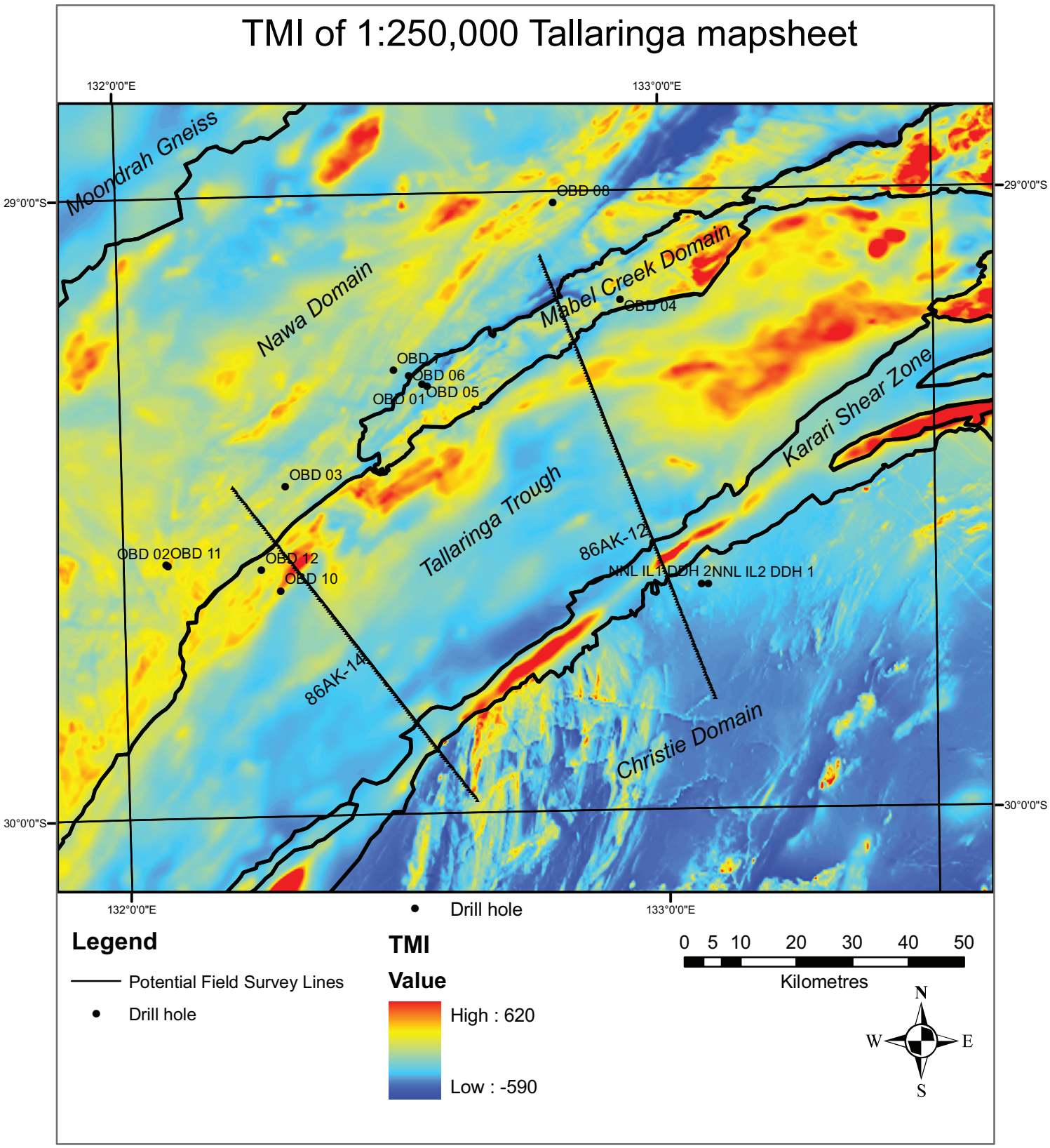

Figure 2: Total Magnetic Intensity (TMI) map of the Tallaringa 1:250,000 map sheet projected in GDA94 MGA Zone 53. Includes the potential field model lines and drill hole positions with respect to magnetic anomalies.

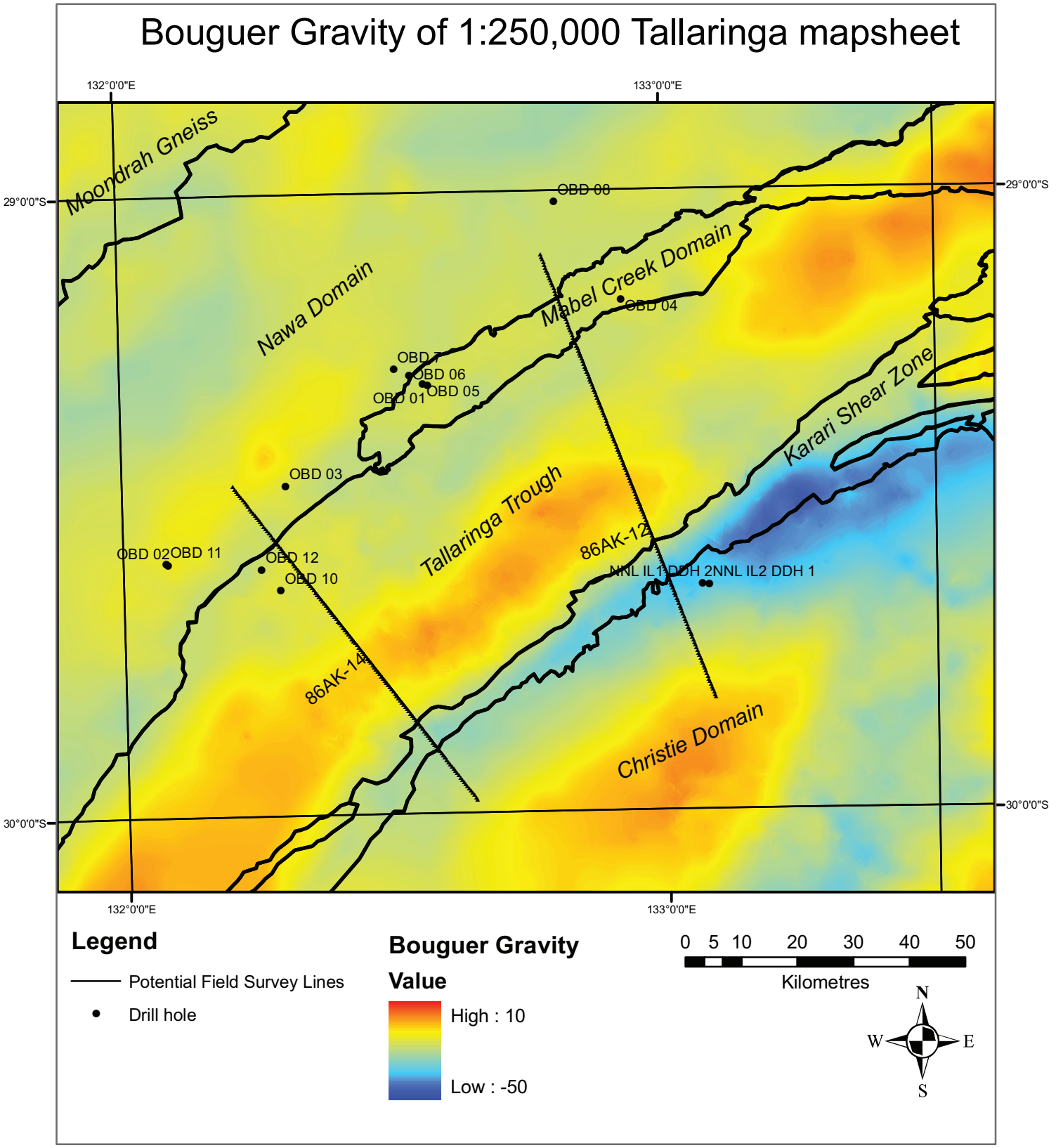

Figure 3: Bouguer Gravity map of the Tallaringa 1:250,000 map sheet projected in GDA94 MGA Zone 53. Includes the potential field model lines and drill hole positions with respect to gravity anomalies.

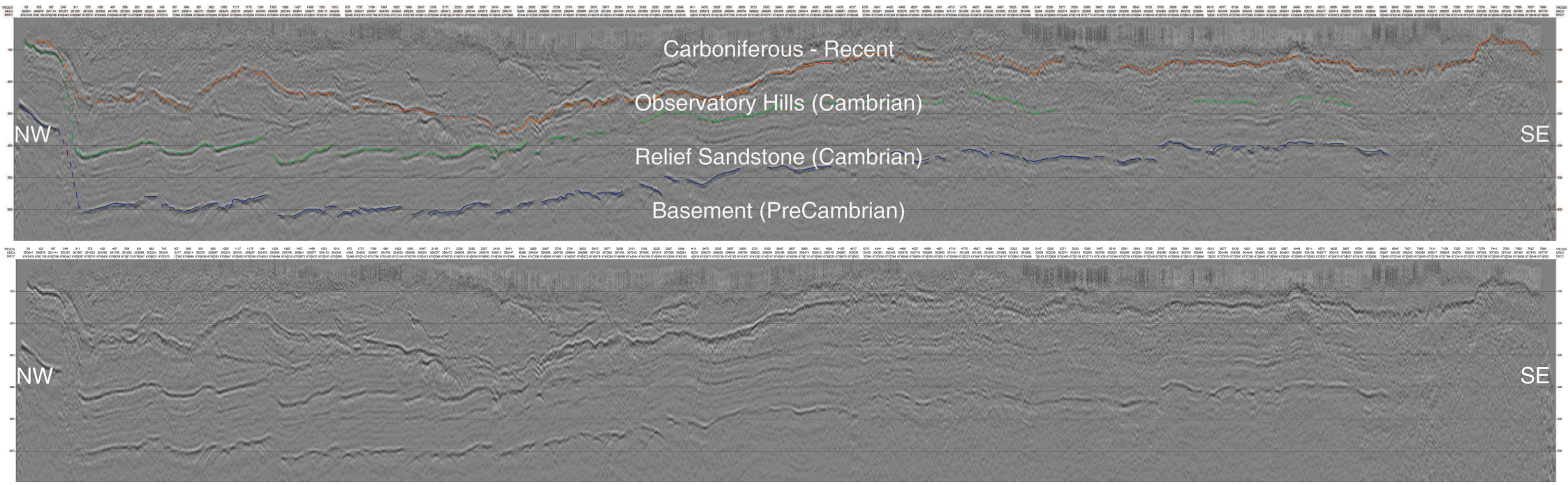

Figure 4a: Seismic reflection and refraction survey 86 AK-12 across Tallaringa Trough. Two way time (msec) versus distance (m). Coloured lines indicate primary reflectors. Stratigraphic interpretation after Cockshell in Benbow (1993).

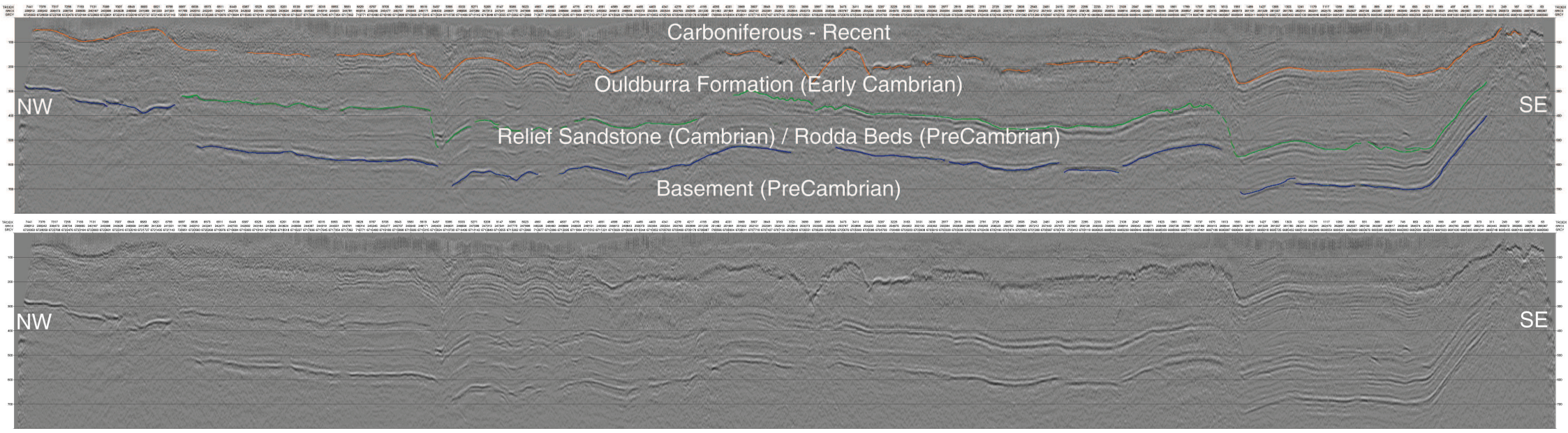

Figure 4b: Seismic reflection and refraction survey 86 AK-14 across Tallaringa Trough. Two way time (msec) versus distance (m). Coloured lines indicate primary reflectors. Stratigraphic interpretation after Cockshell in Benbow (1993).

Tallaringa Gravity Stations and Aeromagnetic Survey Coverage

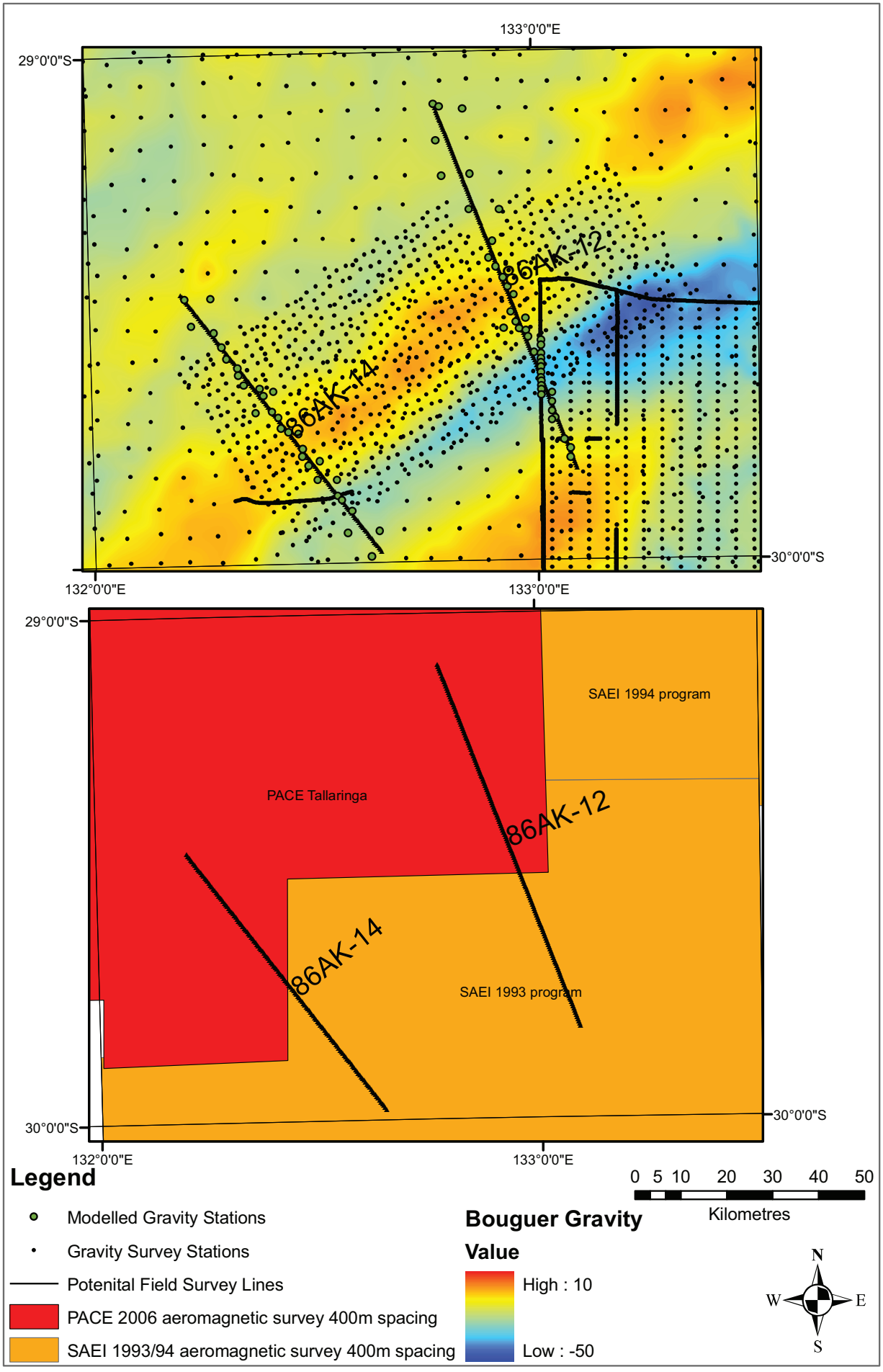

Figure 5: Maps of gravity survey stations and aeromagnetic surveys conducted within the Tallaringa map sheet. Green, larger dots indicate gravity stations chosen by closest perpendicular distance to the potential field modelled lines. Both maps are projected in GDA94 MGA Zone 53

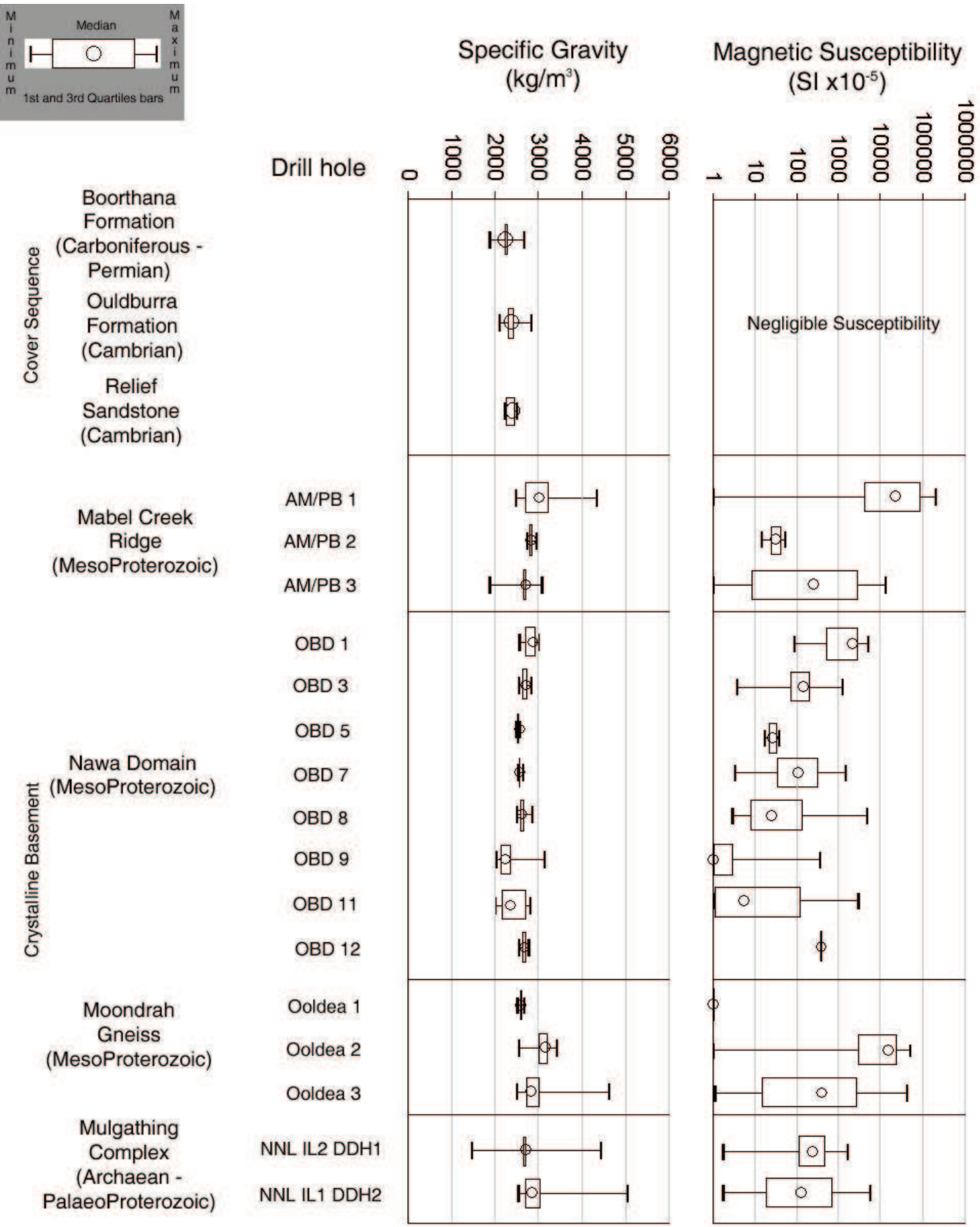

Figure 6: Petrophysical statistical comparison of drill core from the western Gawler Province.

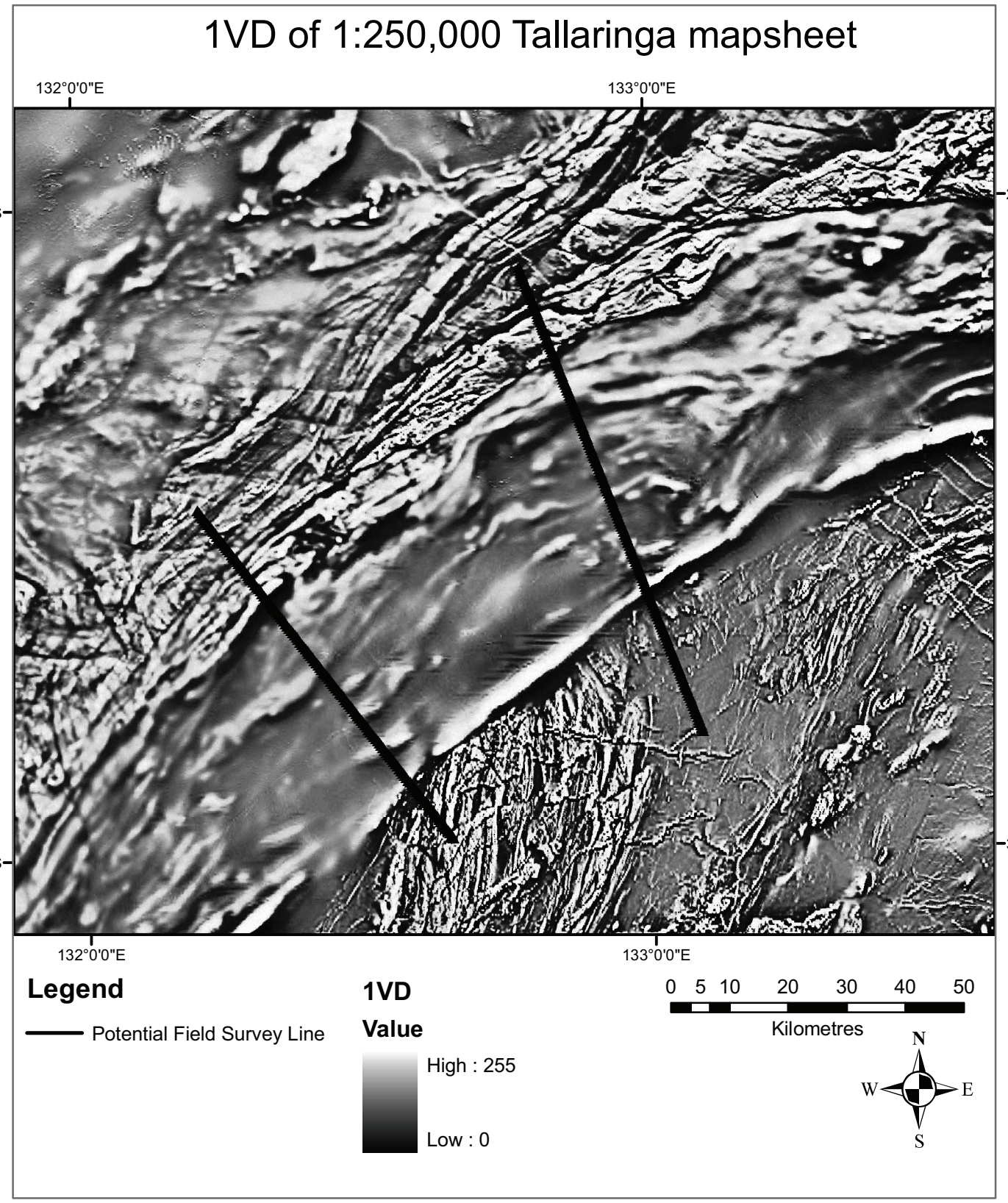

Figure 7: First Vertical Derivative (1VD) of the Tallaringa map sheet, projected in GDA94 MGA Zone 53.

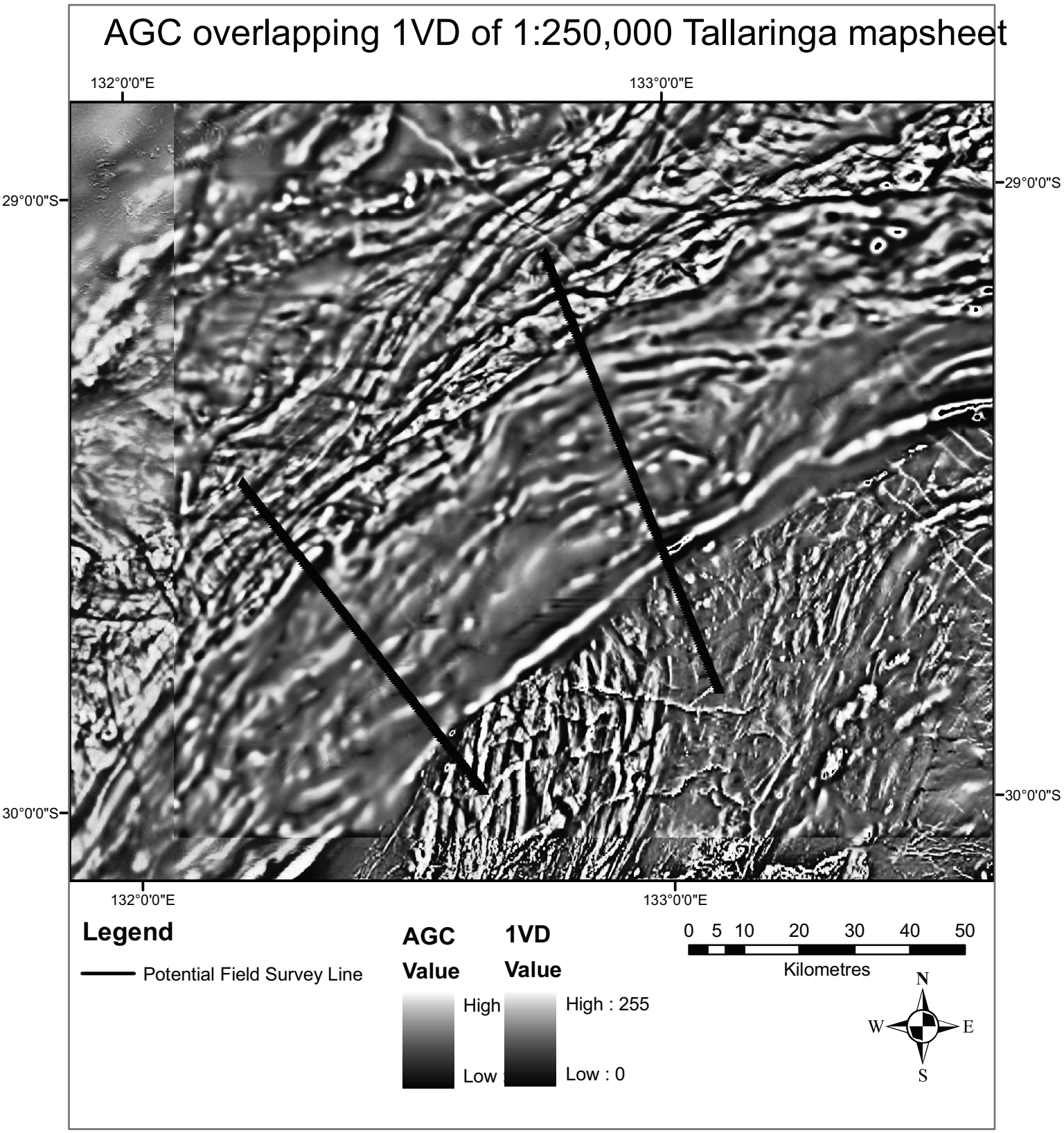

Figure 8: Automatic Gain Control (AGC) of the 1VD overlaying the 1VD of the Tallaringa map sheet, projected in GDA94 MGA Zone 53. Note the discordance where high detailed anomalies in 1VD have been smoothed by AGC to "equalise" with lower frequency anomalies of the study area.

Tilt of RTP of 1:250,000 Tallaringa mapsheet

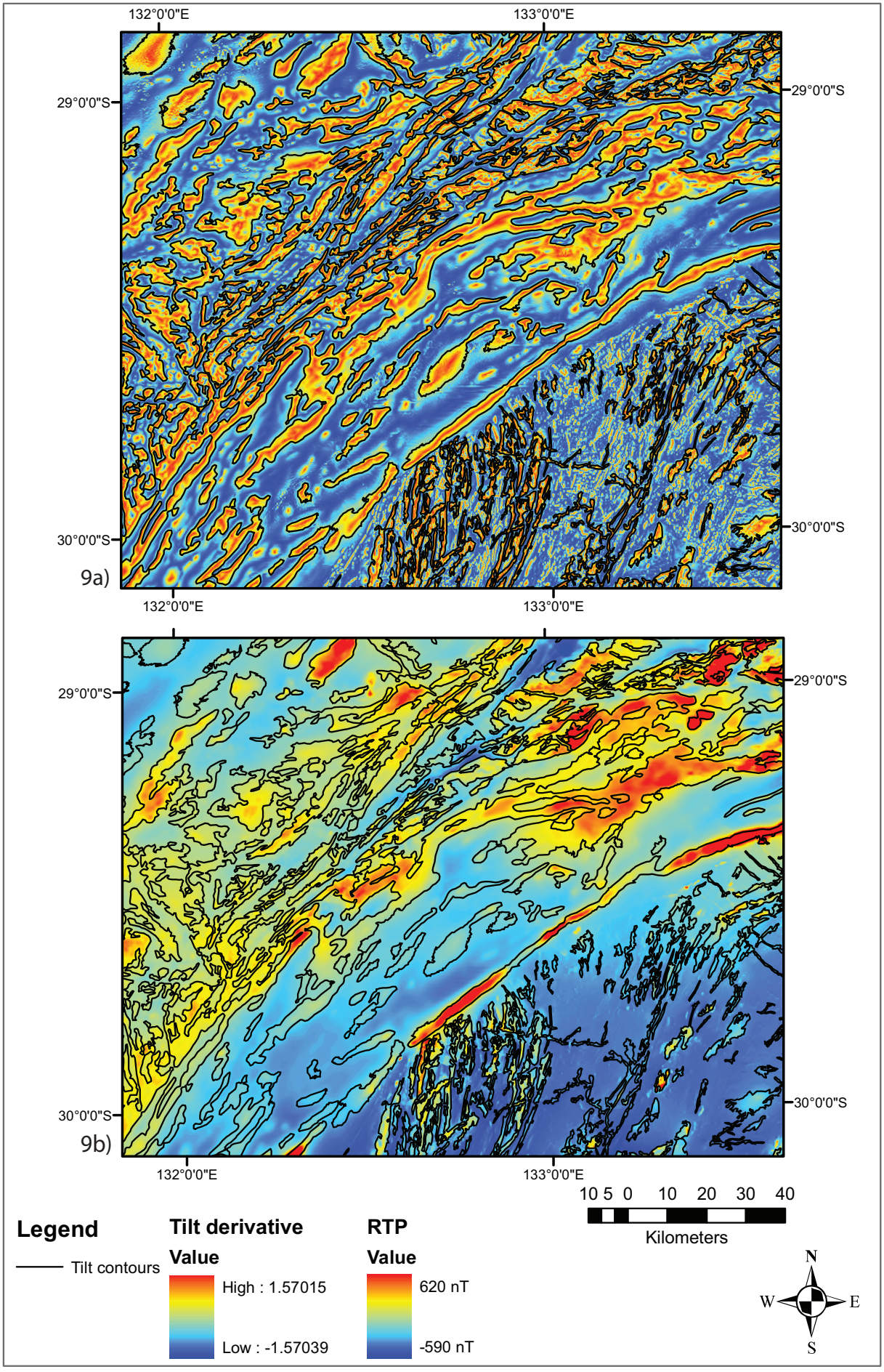

Figure 9a: Tilt derivative of the Reduced To Poles (RTP) map with automatic contouring in Oasis Montaj where the tilt derivative = 0.

Figure 9b: The Reduced to Poles (RTP) overlain with the above contour lines to compare the detected edges of continuous magnetic bodies with a map typically used to delineate edges by visual recognition.

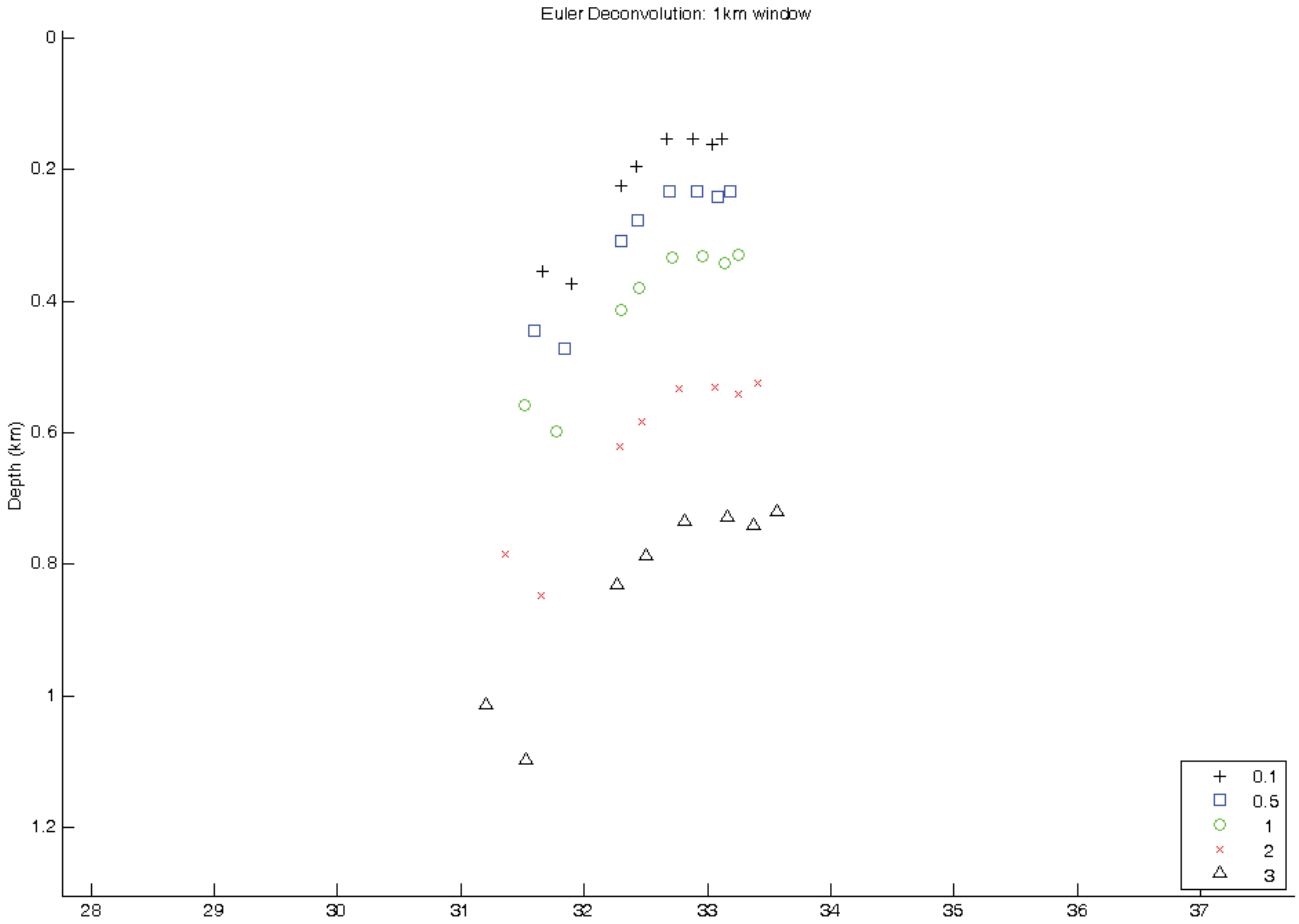

Figure 10: Euler Deconvolution generated in Matlab from the TMI of the 86AK-14 traverse demonstrating that depth to source estimates of the technique are related to the structural index . There is approximately 1km of difference between the shapes that can generate the TMI field within the 31 - 34 km range.

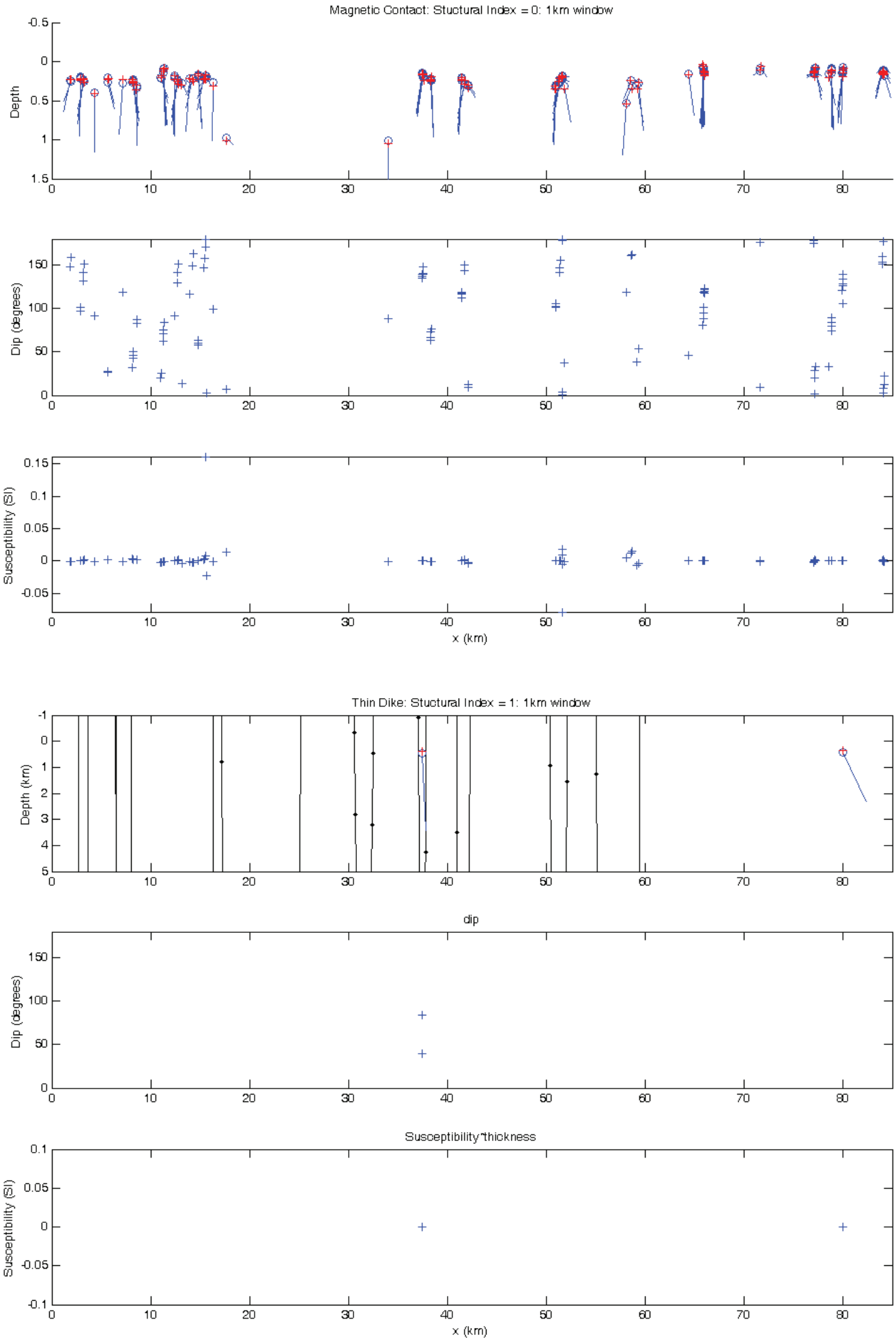

Figure 11: Extended Euler Deconvolution results for profile 86AK-12 for a 1 km window. Top displays detected the positions for (SI = 0) magnetic contacts, their depth, angle of dip and susceptibilty contrast. Bottom displays detected positions for SI = 1 (dike like structures), their dip angle and susceptibilty x thickness.

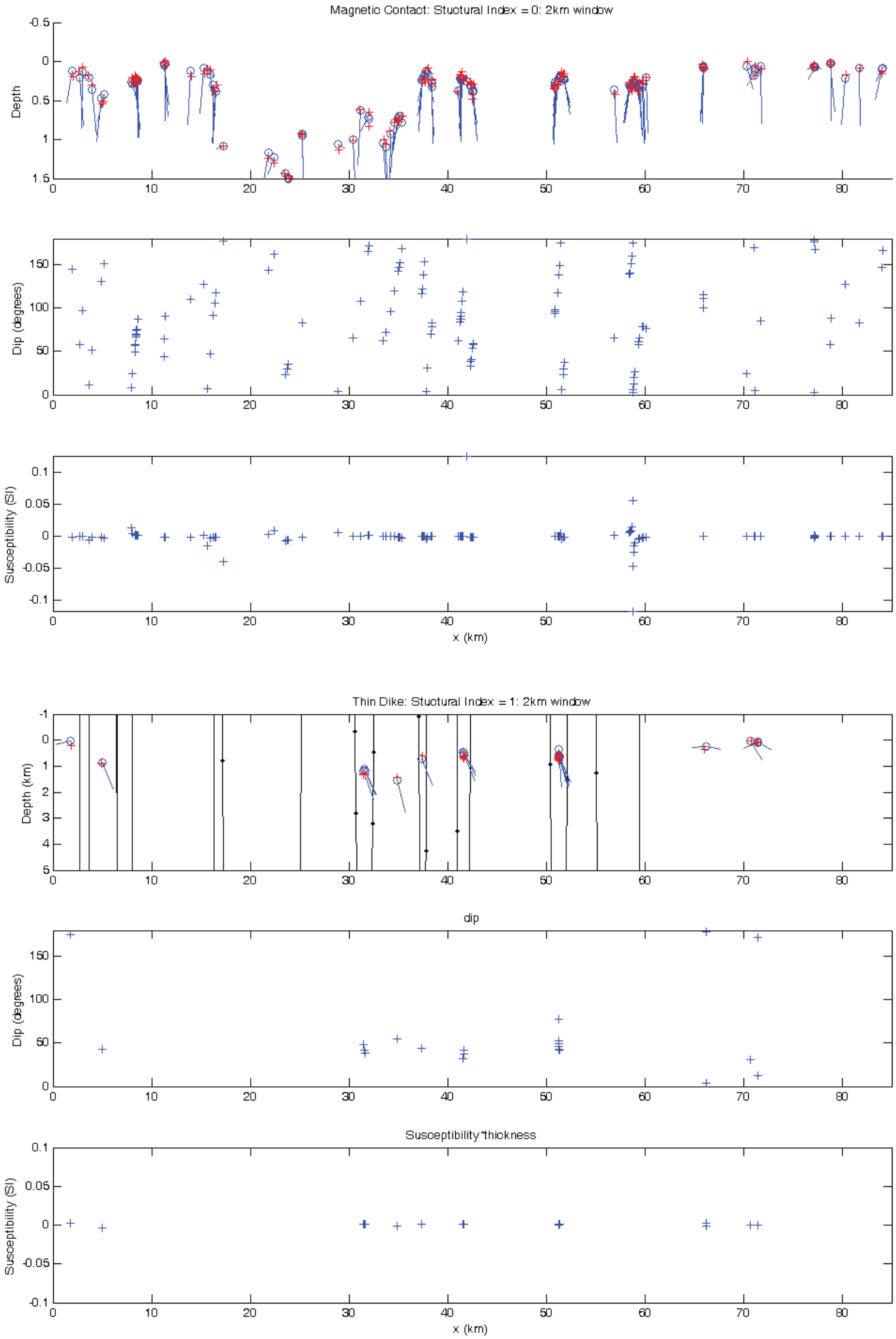

Figure 12: Extended Euler Deconvolution results for profile 86AK-12 for a 2 km window. Top displays detected the positions for (SI = 0) magnetic contacts, their depth, angle of dip and susceptibilty contrast. Bottom displays detected positions for SI = 1 (dike like structures), their dip angle and susceptibilty x thickness.

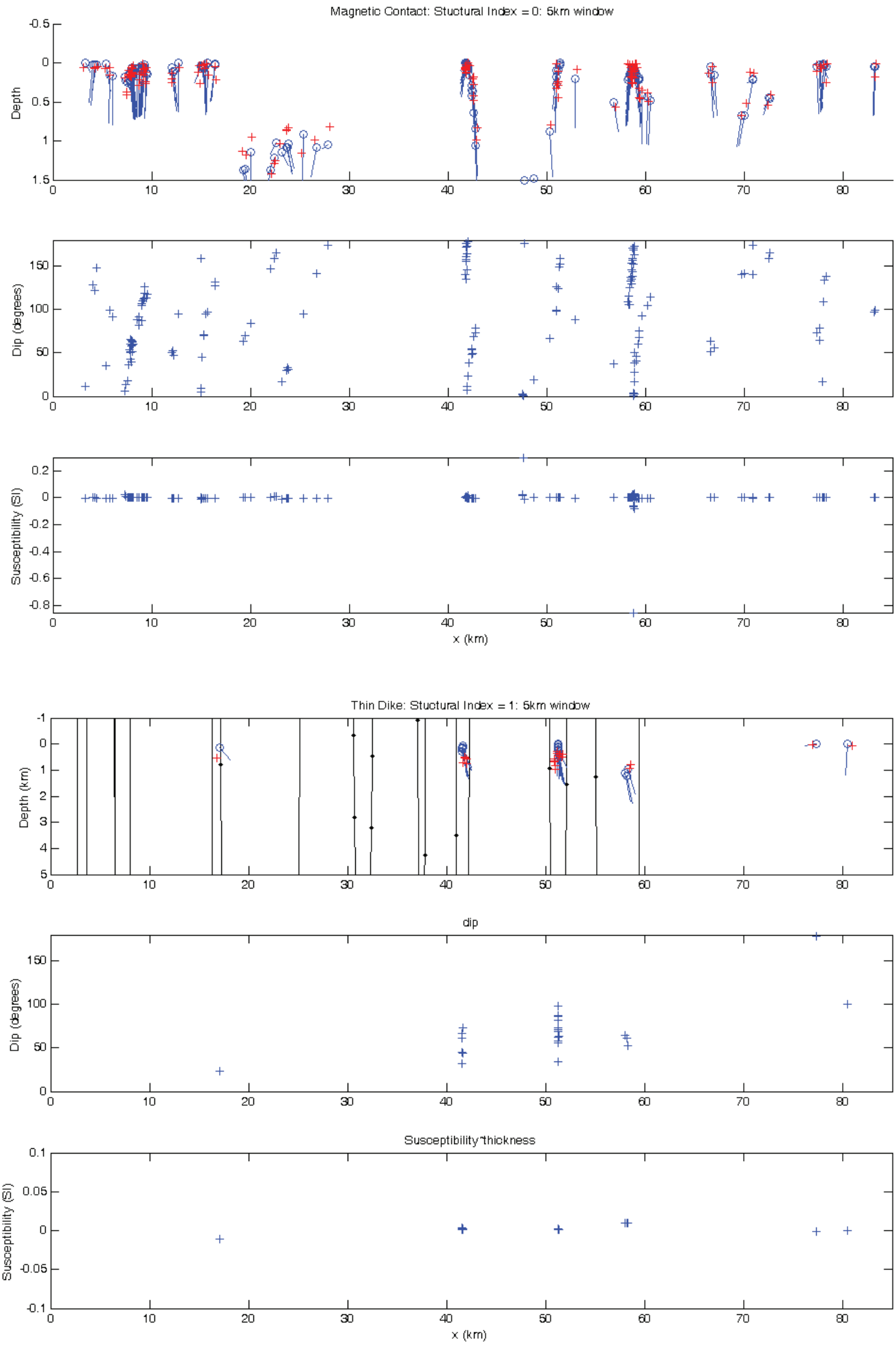

Figure 13: Extended Euler Deconvolution results for profile 86AK-12 for a 5 km window. Top displays detected the positions for (SI = 0) magnetic contacts, their depth, angle of dip and susceptibilty contrast. Bottom displays detected positions for SI = 1 (dike like structures), their dip angle and susceptibilty x thickness.

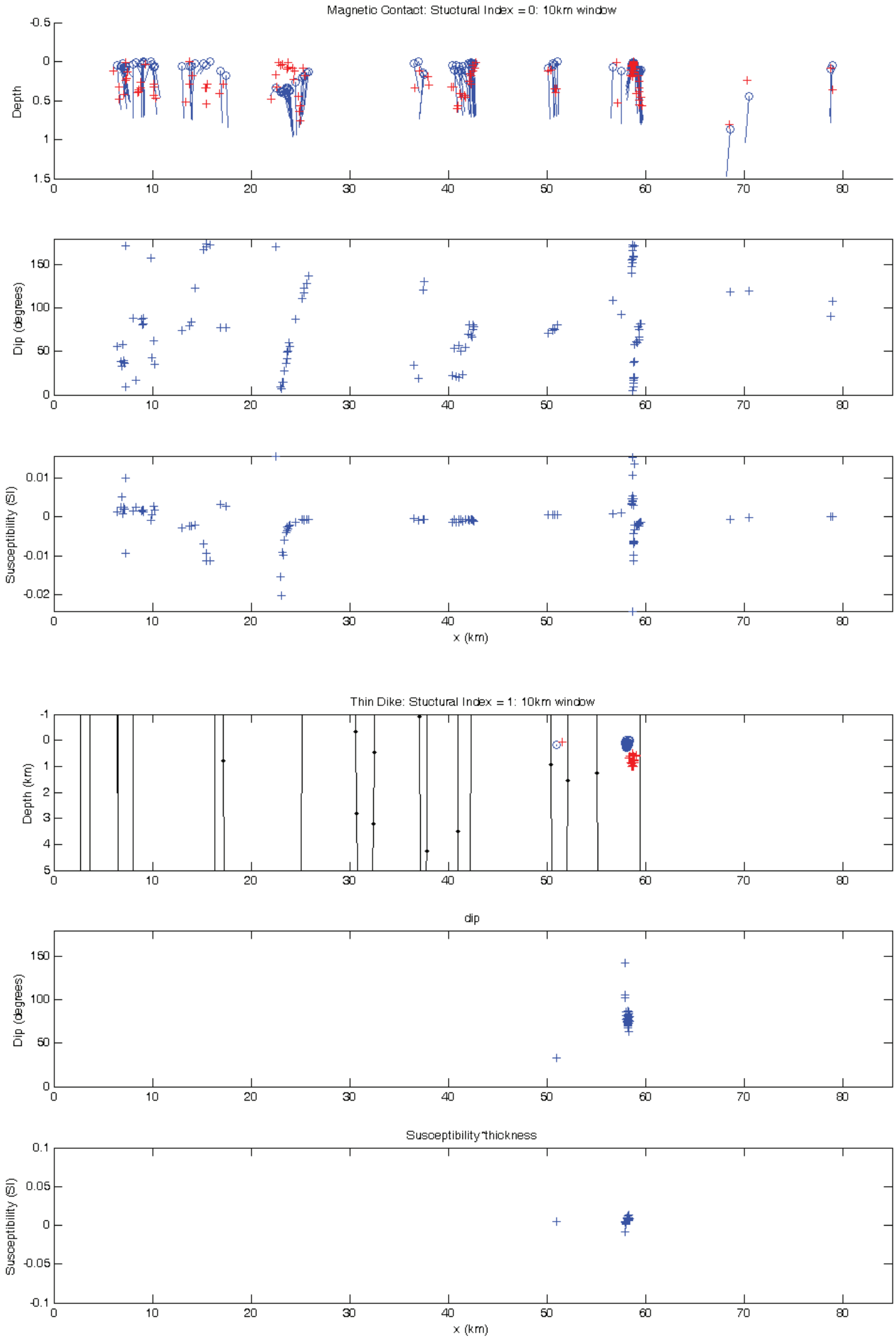

Figure 14: Extended Euler Deconvolution results for profile 86AK-12 for a 10 km window. Top displays detected the positions for (SI = 0) magnetic contacts, their depth, angle of dip and susceptibilty contrast. Bottom displays detected positions for SI = 1 (dike like structures), their dip angle and susceptibilty x thickness.

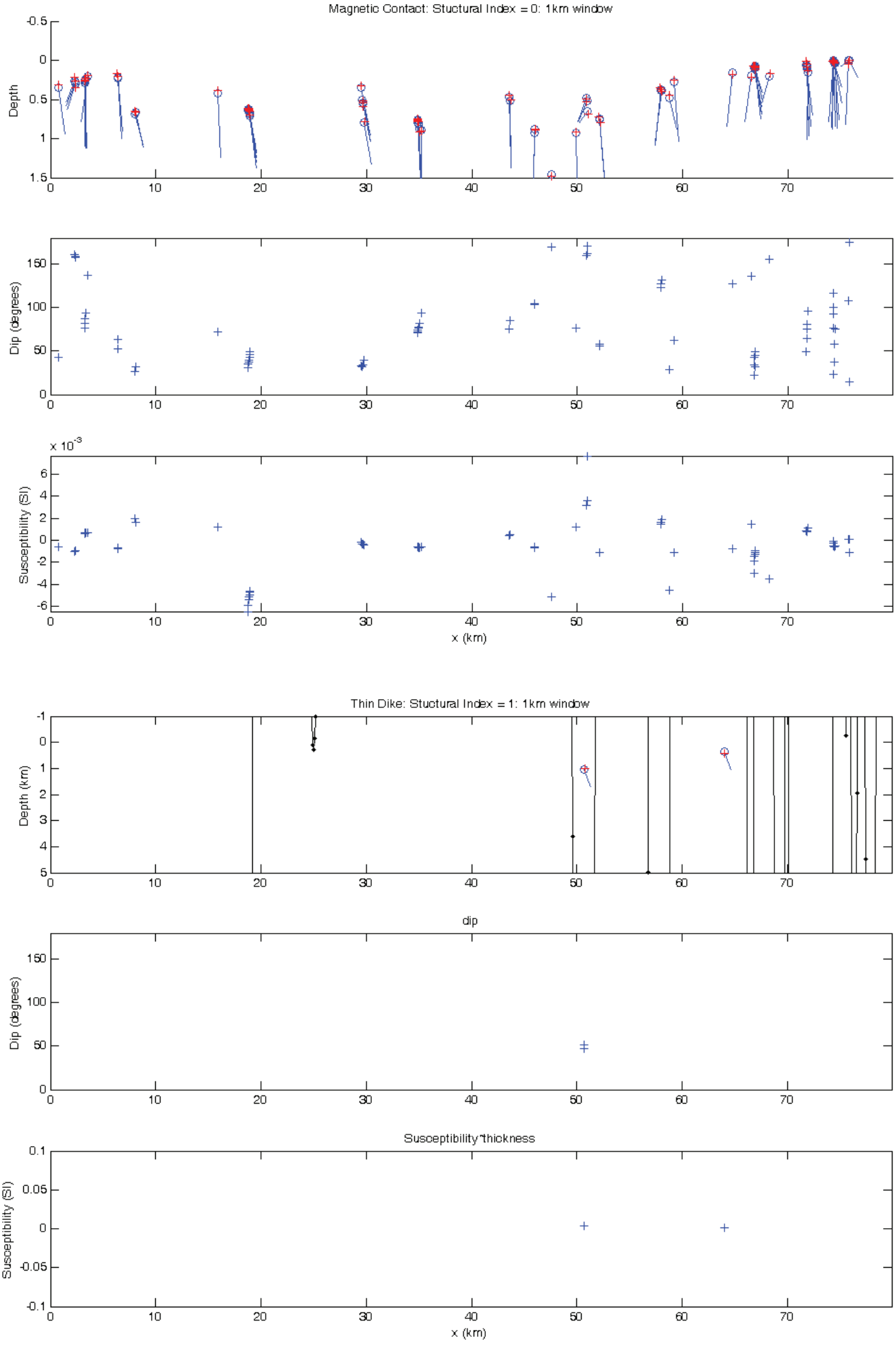

Figure 15: Extended Euler Deconvolution results for profile 86AK-14 for a 1 km window. Top displays detected the positions for (SI = 0) magnetic contacts, their depth, angle of dip and susceptibilty contrast. Bottom displays detected positions for SI = 1 (dike like structures), their dip angle and susceptibilty x thickness.

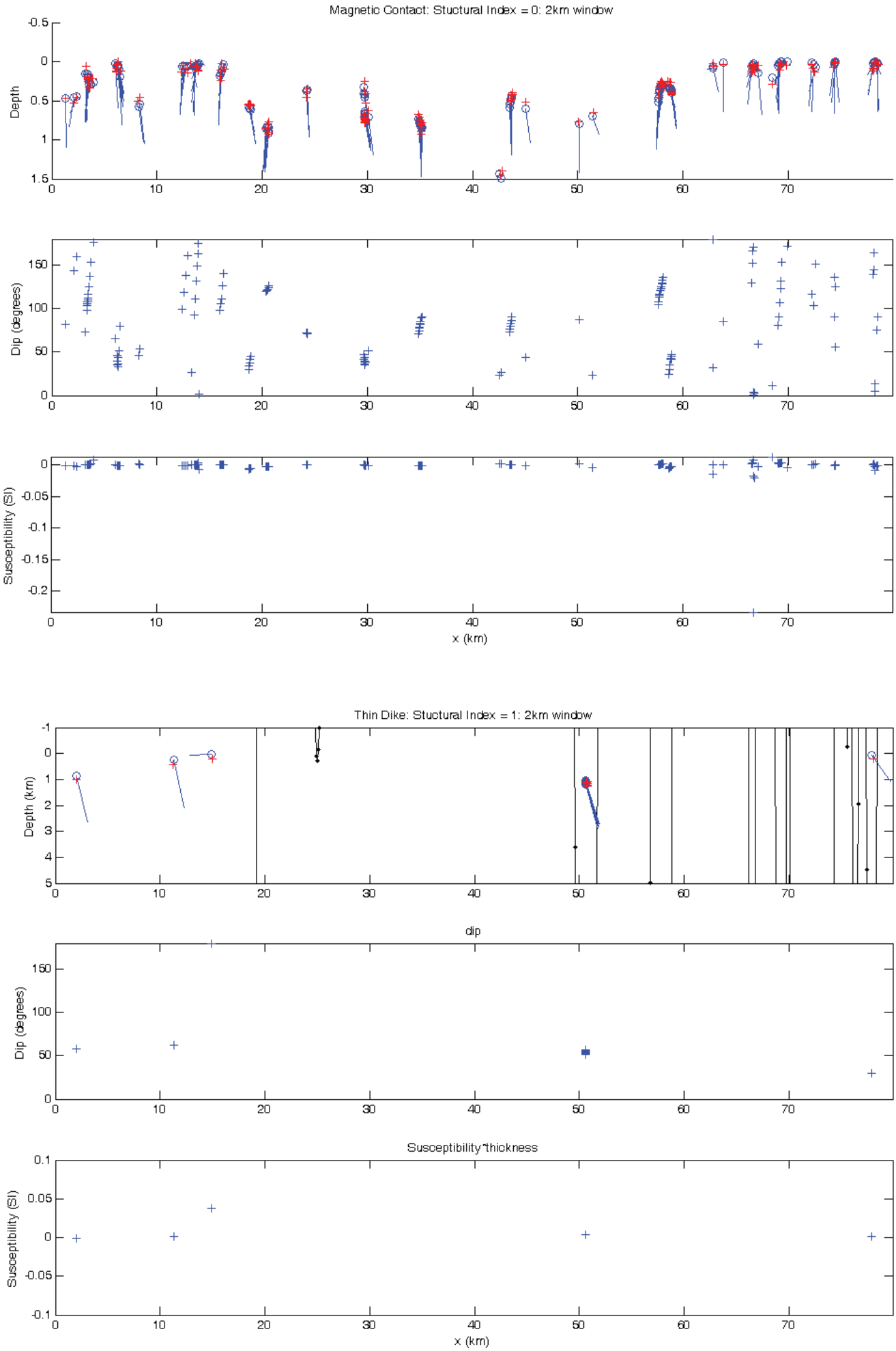

Figure 16: Extended Euler Deconvolution results for profile 86AK-14 for a 2 km window. Top displays detected the positions for (SI = 0) magnetic contacts, their depth, angle of dip and susceptibilty contrast. Bottom displays detected positions for SI = 1 (dike like structures), their dip angle and susceptibilty x thickness.

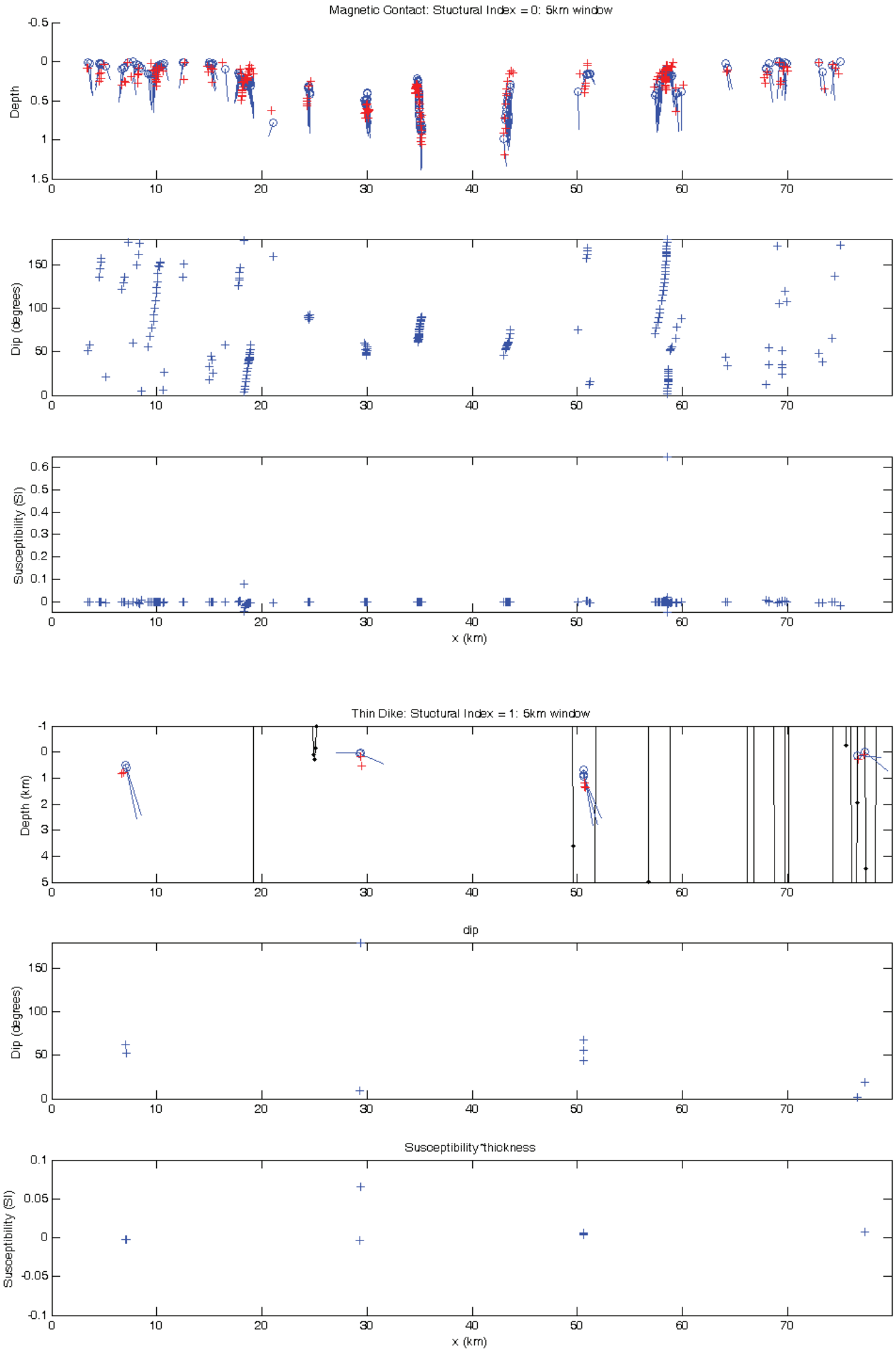

Figure 17: Extended Euler Deconvolution results for profile 86AK-14 for a 5 km window. Top displays detected the positions for (SI = 0) magnetic contacts, their depth, angle of dip and susceptibilty contrast. Bottom displays detected positions for SI = 1 (dike like structures), their dip angle and susceptibilty x thickness.

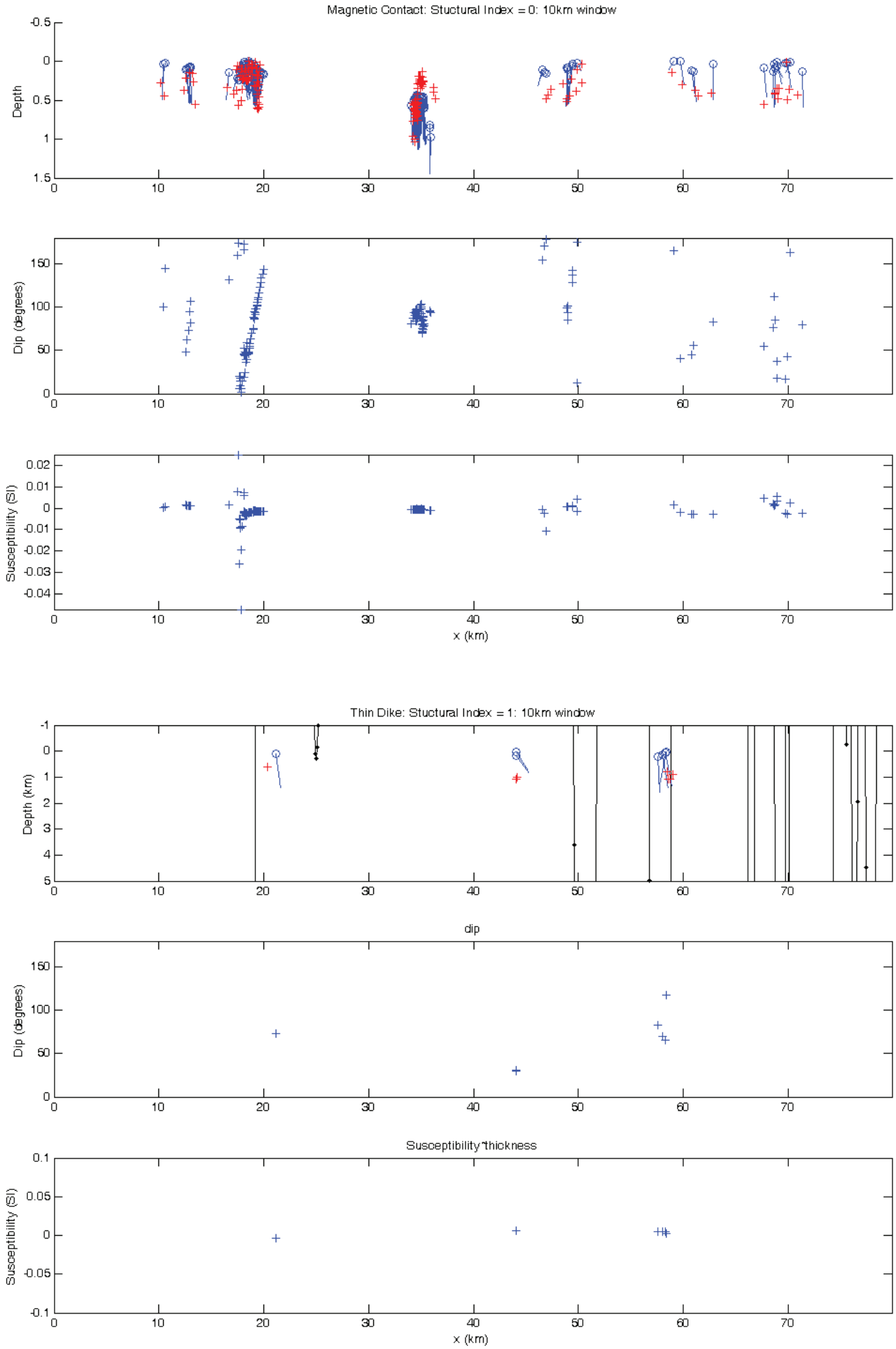

Figure 18: Extended Euler Deconvolution results for profile 86AK-14 for a 10 km window. Top displays detected the positions for (SI = 0) magnetic contacts, their depth, angle of dip and susceptibilty contrast. Bottom displays detected positions for SI = 1 (dike like structures), their dip angle and susceptibilty x thickness.

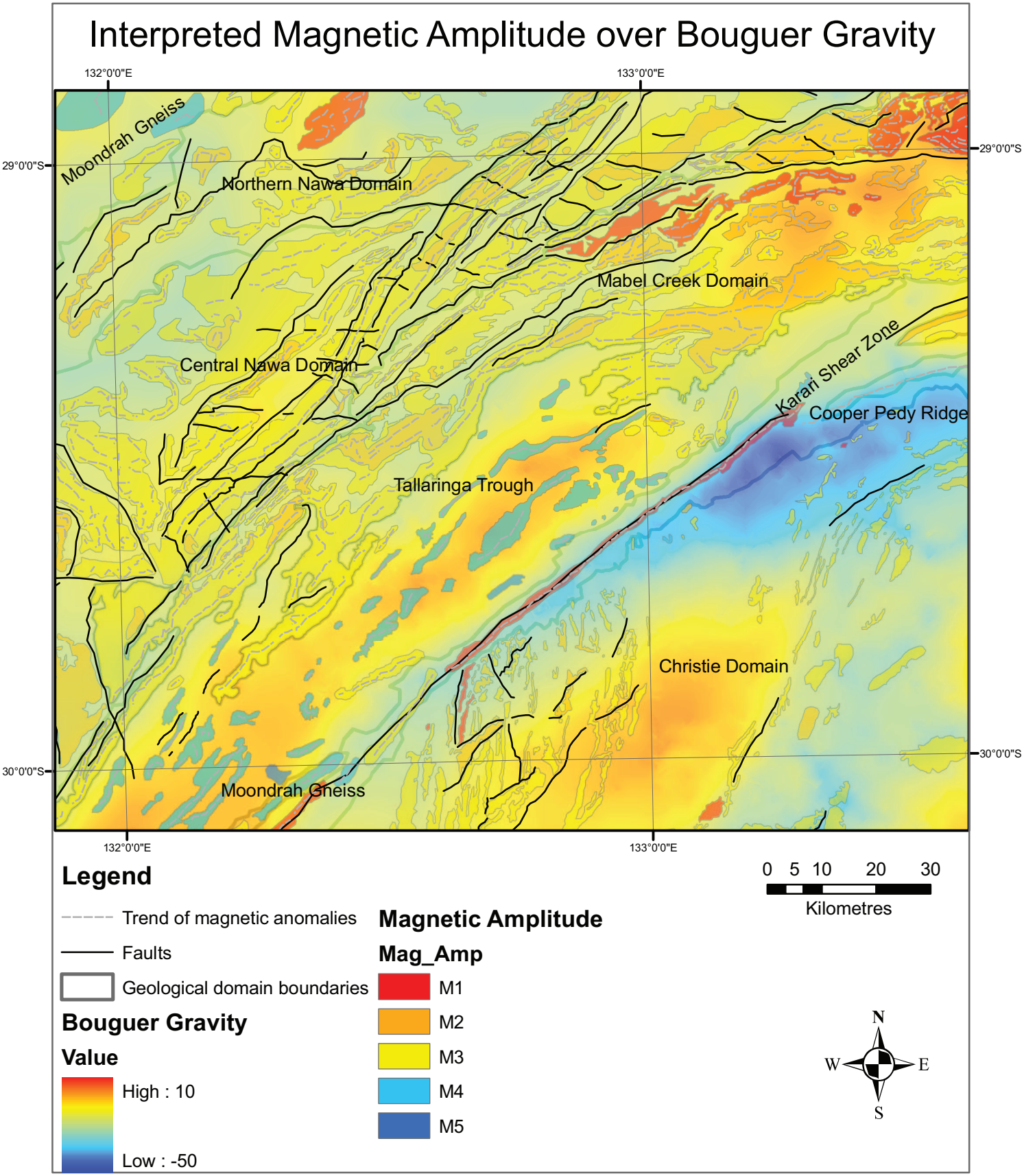

Figure 19: Geophysical interpretation of magnetic bodies over the Bouguer Gravity map of the Tallaringa mapsheet, projected in GDA94 MGA Zone 53. Bodies are coloured by magnetic amplitude to display the changing association of magnetism with gravity between domains.

Geophysical interpretation of Tallaringa 1:250k map sheet

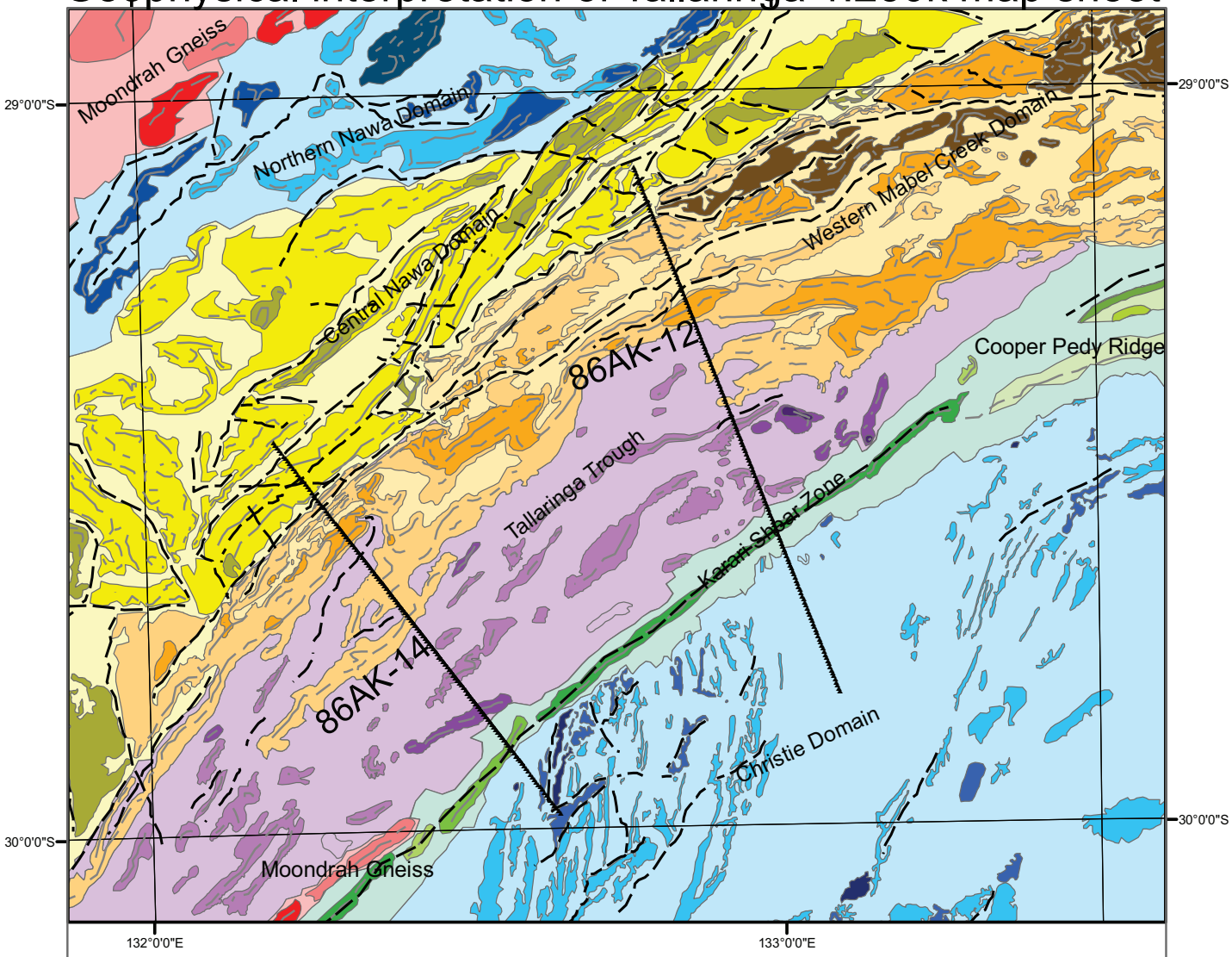

Cooper Pedy Ridge

Highly magnetic domain to the north east slightly intruding the map sheet. Moderate magnetic, low density anomalies in alignment with the KSZ.

- Strongly - moderately magnetised
- Moderately magnetised

Northern Nawa Domain

Large magnetic range and lack of a regional vector to anomaly alingments.Generally deep wavelengths due to overlying Officer Basin.

- Strongly magnetised
- Strongly - moderately magnetised
- Moderately magnetised
- Moderately - weakly magnetised

Central Nawa Domain

Moderate - strong magnetics in diffusely banded, occasionally sinuous textured and moderately deep anomalies. Moderate gravity.

- Strongly - moderately magnetised
- Moderately magnetised

Western Mabel Creek Ridge

High - moderate magnetism, detailed textures diffuse south into the trough, shallow to moderate depth anomalies, moderate - low gravity.

- Strongly magnetised
- Strongly - moderately magnetised
- Moderately magnetised

Tallaringa Trough

Moderate - weakly magnetised area of deep, diffuse anomalies. High gravity comparable with Mabel Creek or Moondrah Domains. Bland anomalies and NE-SW lineaments.

- Moderate - weakly magnetised
- Moderately magnetised
- Moderately - weakly magnetised
- Reversed magnetics (possible intrusion)

Moondrah Gneiss

Moderately magnetic in the map sheet, diffuse texures. Moderate - high density and overall deeper anomalies.

- Strongly - moderately magnetised
- Moderately magnetised
- Weak - moderate magnetised

Karari Shear Zone

Bland, strongly magnetic shear zone. Very low density.

- Strong, bland magnetised
- Moderately magnetised
- Weak - moderate magnetised

Christie Domain

Shallow metasediments with banded, linear texture and moderate magnetisation with mottled, high magnetic intrsuions

- Strongly magnetised
- Moderate - strongly magnetised
- Moderately magnetised
- Weakly magnetised

Potential Field Survey Line

Faults

Trend of magnetic anomalies

N W E S

0 5 10 20 30

Kilometres

Figurer 20: Geophysical interpretation of the Tallaringa map sheet, projected in GDA94 MGA Zone 53.

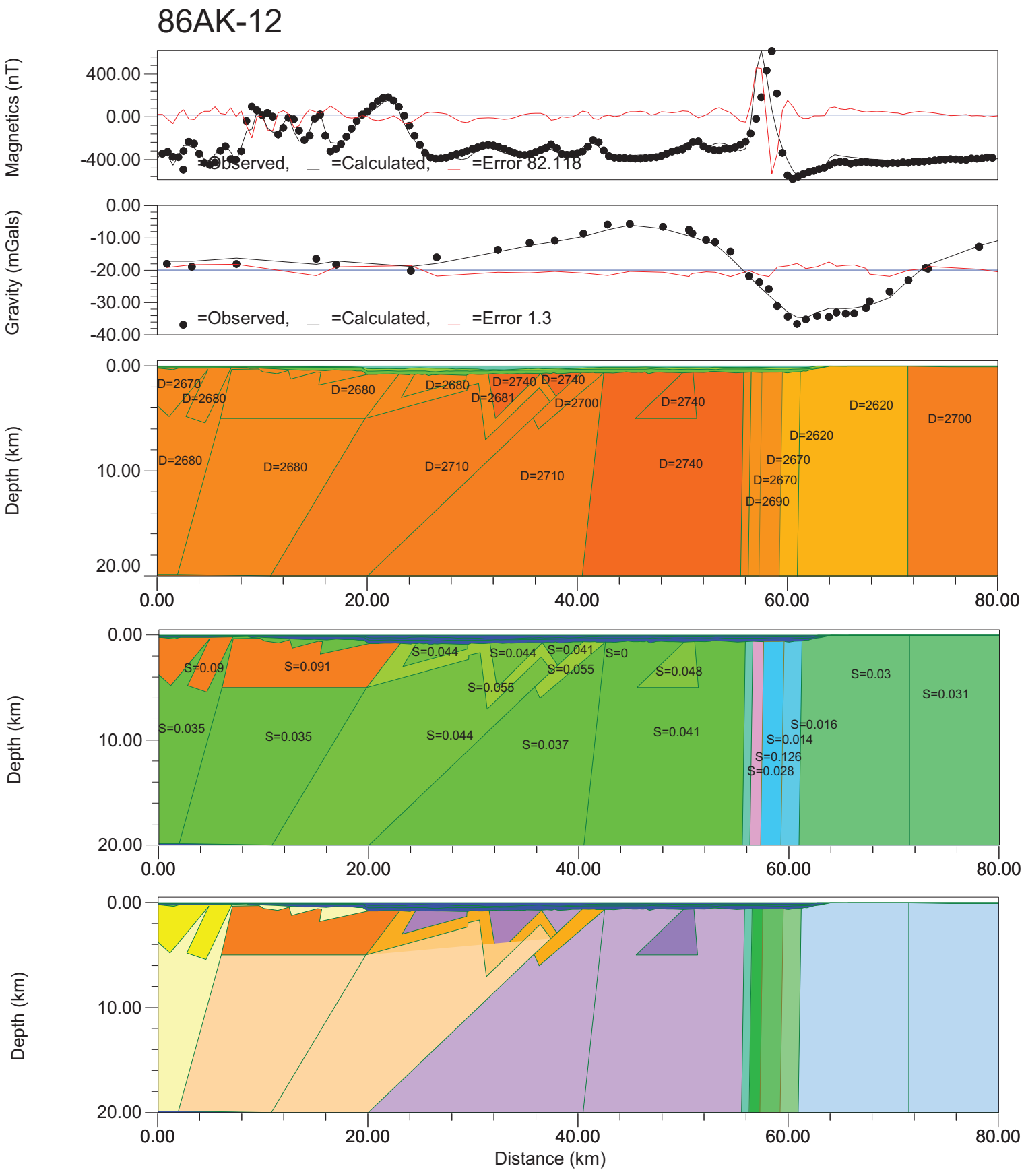

Figure 21: Forward model of potential filed profile 86AK-12 displaying density values for blocks. Density Shading uses a the colour spectrum stretched between 2000 - 3000 kgm-3. Magnetic susceptibility is stretched between 0 and 1.25 SI. The base figure colours correlate to the geophysical domain interpretations in figure 20.

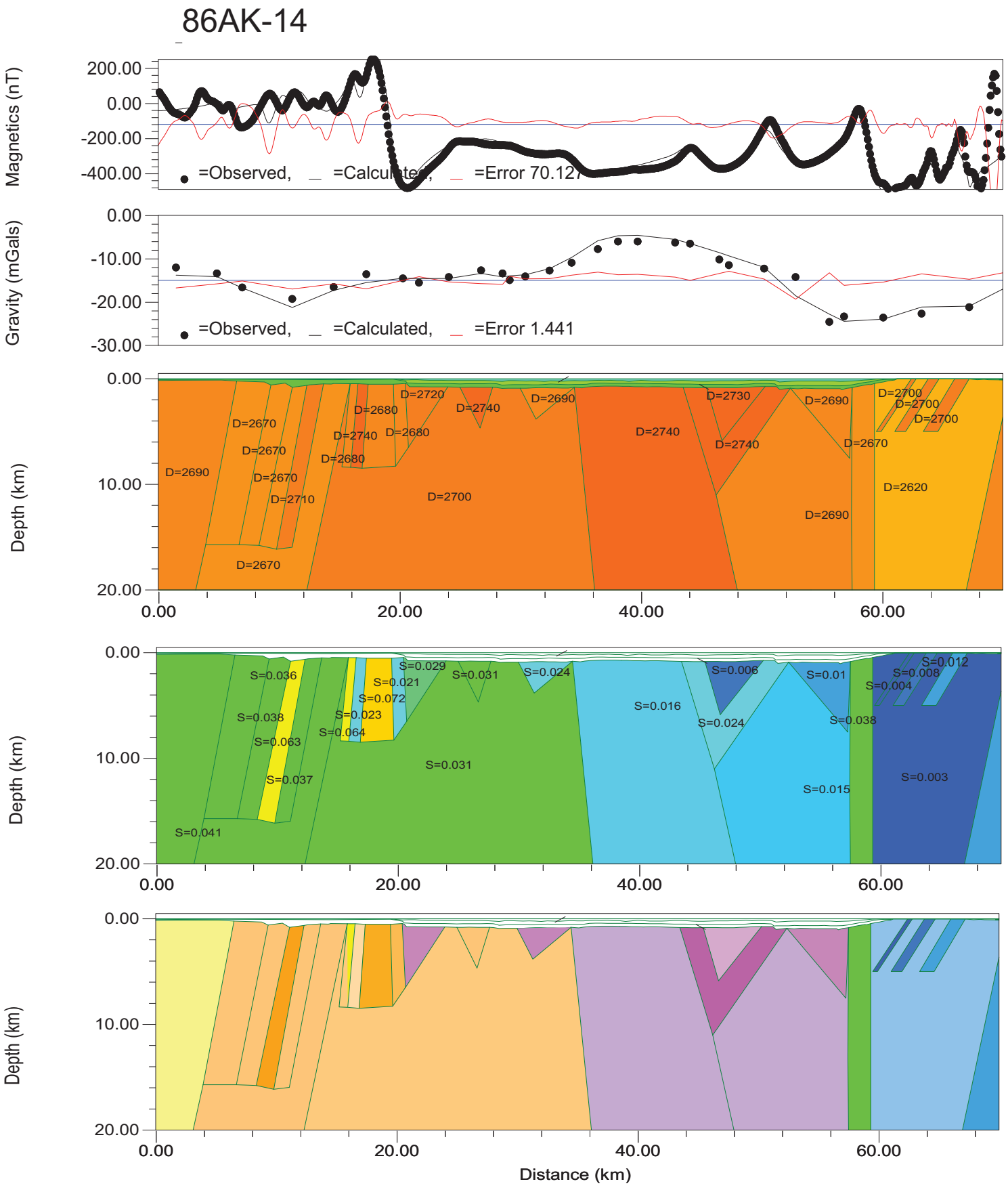

Figure 22: Forward model of potential filed profile 86AK-12 displaying density values for blocks. Density Shading uses a the colour spectrum stretched between 2000 - 3000 kgm-3. Magnetic susceptibility is stretched between 0 and 1.25 SI. The base figure colours correlate to the geophysical domain interpretations in figure 20.